NASA CONTRACTOR REPORT

NASA CR-61337

A MAXOMETER FOR PEAK WIND SPEED ANEMOMETERY

By P. T. Johnson and M. C. Krause

Lockheed Missile and Space Company
Huntsville Research Park
4800 Bradford Drive
Huntsville, Alabama

June 1970

Final Report

Prepared for

NASA-GEORGE C. MARSHALL SPACE FLIGHT CENTER
Marshall Space Flight Center, Alabama 35812

TECHNICAL REPORT STANDARD TITLE PAGE

1. REPORT NO.	2. GOVERNMENT ACCESSION NO.	3. RECIPIENT'S CATALOG NO.
NASA CR-61337		

4. TITLE AND SUBTITLE	5. REPORT DATE
A MAXOMETER FOR PEAK WIND SPEED ANEMOMETRY	June 1970
	6. PERFORMING ORGANIZATION CODE
7. AUTHOR(S) P. T. Johnson and M. C. Krause	8. PERFORMING ORGANIZATION REPORT #
9. PERFORMING ORGANIZATION NAME AND ADDRESS Lockheed Missile & Space Company Huntsville Research Park 4800 Bradford Drive Huntsville, Alabama	10. WORK UNIT NO. 11. CONTRACT OR GRANT NO. NAS8-24020 13. TYPE OF REPORT & PERIOD COVERED Contractor Report Final
12. SPONSORING AGENCY NAME AND ADDRESS NASA-George C. Marshall Space Flight Center Aero-Astrodynamics Laboratory Marshall Space Flight Center, Alabama 35812	14. SPONSORING AGENCY CODE

15. SUPPLEMENTARY NOTES

16. ABSTRACT

Lockheed has designed, fabricated, and tested a peak wind speed anemometer (Maxometer) under contract to the Marshall Space Flight Center (March 1969 through May 1970 Contract specifications called for a purely mechanical device with anti-spark properties (no metal-to-metal moving contact) capable of measuring winds from 8 meters per second up to 200 meters per second, and then keeping a permanent record of the peak wind. Along with this was the necessity to withstand the Saturn V launch conditions on the Launch Umbilical Tower (2000 degrees F) and an accuracy design goal of ± 5 percent of reading.

A maxometer concept which used a flat disk and two constant-rate springs (high and low) was designed and developed. The concept included a precision clutching mechanism to retain a given displacement of the springs when exposed to the dynamic pressure generated from a given maximum wind velocity, Two maxometer configurations were developed: Models S and E. The Model S configuration was a fixed-orientation model capable of exposure to, and measurement of, winds induced during a typical launch from the Saturn V Launch Umbilical Tower. The Model E configuration was a weather-vaning model which was designed for the normal meteorological environment. The same measuring and recording technique was used in both models.

Three Model S and three Model E Maxometers were fabricated, tested and delivered to the customer. Four of these models, three Model S and one Model E, were tested in the NASA-Langley Research Center 7 x 10-foot wind tunnel. Results of these tests indicate that the Maxometer is capable of meeting the design specification, except for the low-range dynamic pressure values. Wind tunnel tests in the low range were inadequate to

(continued)

17. KEY WORDS	18. DISTRIBUTION STATEMENT PUBLIC RELEASE: E. D. Geissler Director, Aero-Astrodynamics Laboratory

19. SECURITY CLASSIF. (of this report)	20. SECURITY CLASSIF. (of this page)	21. NO. OF PAGES	22. PRICE
UNCLASSIFIED	UNCLASSIFIED	91	

MSFC - Form 3292 (May 1969)

ABSTRACT (concluded)

properly evaluate the low-range characteristics (8 to 30 meters per second) because of limitations of the tunnel facility in the low velocity region. Further field and wind tunnel tests are recommended to properly evaluate the Maxometer over the full range of performance characteristics. Also, minor design changes are recommended to reduce fabrication costs and to relieve potential operational limitations.

FOREWORD

This final report documents the results of a 14-month effort to design, develop, fabricate and test a peak wind speed anemometer, or MAXOMETER, for the NASA-Marshall Space Flight Center's Aero-Astrodynamics Laboratory. This program was conducted by Lockheed Missiles & Space Company's Huntsville Research & Engineering Center (Lockheed/Huntsville). The work was performed under NASA Contract NAS8-24020 during the period 26 March 1969 through 25 May 1970 by Lockheed/Huntsville's Systems Engineering Organization, Mr. A. S. Dunbar, Manager. Wind tunnel tests conducted during the program were done in NASA-Langley Research Center's 7 x 10-foot tunnel facility. All other work was done at Lockheed/Huntsville. Project Engineer was Mr. R. B. Wysor, Supervisor, Systems Engineering Advanced Development Section. Lead Engineer for the design and development efforts was Mr. P. T. Johnson, who was assisted by Messrs. M. C. Krause and N. O. Wages for analysis, calibration and drafting efforts.

Contracting Officer's Representatives for this program were Mr. John W. Kaufman, Principal, and Mr. Dennis W. Camp, Alternate, of NASA-MSFC Aero-Astrodynamics Laboratory, Aerospace Environment Division.

ACKNOWLEDGEMENTS

Appreciation is expressed to Mr. John W. Kaufman and Mr. Dennis W. Camp of the NASA-MSFC's Aero-Astro Aerospace Environment Division for their support and guidance in conducting the development efforts reported herein. Special appreciation is expressed to Mr. Camp for assistance in planning and coordinating the wind tunnel tests at NASA-Langley Research Center, and to Messrs. W. W. Vaughan and Robert E. Turner for their guidance during concept development and critique of this final report. Also, the assistance of the following NASA-Langley Research Center personnel in conducting the wind tunnel tests is gratefully acknowledged:

H. G. Wiley	Section Head, Vehicle Dynamics Section
E. E. Davenport	Engineer
Jack Smith	Tunnel Mechanic
Hazel Redding	Data Recording
Willis Cross	Photographer

CONTENTS

CONTENTS (Continued)

LIST OF TABLES

LIST OF ILLUSTRATIONS

LIST OF ILLUSTRATIONS (Continued)

NOMENCLATURE

A	area
A_d	area of disk (ft^2)
A_p	area of piston (ft^2)
A_r	area, effective receiving (cm^2)
AR	aspect ratio (dimensionless)
a	spring constant (lb/ft^2 – nonlinear spring) (kg/m^2)
b	span ft (m)
C_d	drag coefficient (dimensionless)
C_o	orifice coefficient (dimensionless)
c	sound velocity (cm/sec)
D_o	orifice diameter (ft)
D_p	piston diameter (ft)
E	modulus of elasticity (lb/in^2)
E_s	sound intensity ($erg/cm^2/sec$)
F	force
F_s	force, spring
g	gravitational constant (ft/sec^2) (m/s^2)
I	inertia ($in\text{-}lb\text{-}sec^2$)
K	spring constant (lb-ft – for linear)
ℓ	moment arm (ft)
M	mass of moving parts ($lb\text{-}sec^2/ft^4$)

P	ambient pressure (lb/ft^2)
P_s	static pressure ($dynes/cm^2$)
q	dynamic pressure (lb/ft^2)
R	universal gas constant ($ft\text{-}lb/lb\text{-}^oF$)
Re	Reynold's number (dimensionless)
r	rainfall (in/min)
S	stress (lb/in^2)
S_c	compressive stress (lb/in^2)
S_f	fin area (ft^2)
T	temperature (^oR) (^oK)
V	velocity (ft/sec or m/sec)
x	system displacement (ft or m)
$\dot{x}$	system velocity (ft/sec or m/sec)
$\ddot{x}$	system acceleration (ft/sec^2 or m/s^2)

Greek

α	coefficient of thermal expansion ($in./in.\text{-}^oF$)
α^o	angle of attack
δ	increase due to thermal expansion (in.)
δ_r	damping ratio
η	velocity resolution error ratio
λ	wavelength (acoustic)
λ_N	wavelength (ft/cycle) or (m/cycle)
μ	friction coefficient 0.2
ν	Poisson's ratio
ρ	density ($lb\text{-}sec^2/ft^4$)

σ	logarithmic decrement
τ	period
ω_N	natural frequency (Hz)

Section 1
INTRODUCTION

The capability of measuring extreme flow conditions in the near vicinity of space vehicles when static tested before and during launch is of major interest to fluid dynamicists, space vehicle engineers and meteorologists. Anemometers presently available for measuring peak wind speeds are not designed to withstand the associated vehicle-induced extreme environmental conditions, such as high flow rates and high temperatures. Conventional anemometers are destroyed under such conditions. In addition to the normal ambient wind flow about space vehicles, measurement of the flow induced by the vehicle engines is desired. Work to date in this area has been primarily theoretical; i.e., by use of the equations of continuity and potential flow theory. The lack of an anemometer capable of measuring extreme wind speeds also impedes the acquisition of data associated with hurricanes, tornadoes, severe thunderstorms, dust devils, etc. Thus, such an anemometer would be beneficial to atmospheric scientists and meteorologists in investigations of extreme wind conditions.

Conventional anemometers have been installed at each of the Saturn vehicle launch pads at Kennedy Space Center. These wind sensors are positioned in such a manner that they will obtain representative ambient horizontal wind data so that conditions can be determined prior to and during vehicle launches. They must, however, be located significant distances from the vehicle so that they will not be damaged or destroyed by the extreme induced flow and temperatures created by vehicle exhaust during launch. Under the terms of this contract, Lockheed developed a Maxometer (Model S) that is designed to monitor the peak winds in the vicinity of space vehicle launch towers and surrounding terrain. Winds to be measured include the induced winds from space vehicle launch and wind conditions caused by natural phenomena such as storms, hurricanes, etc. The Maxometer is capable of measuring the

peak induced winds during the launch phase and maintaining a recording of this reading after the Maxometer has been exposed to the induced flow near the rocket engine exhaust. The Maxometer is reusable with a minimum of refurbishment. In addition to the Model S Maxometer for use in severe launch environments, a Model E Maxometer has been designed and developed for use in normal environmental conditions. This model includes weather-vaning capabilities to measure the peak wind speed regardless of direction.

This report describes the design, development and testing efforts involved in the Maxometer program. Maxometer specifications which were used for guiding these efforts are presented in Section 2. Section 3 describes the design efforts, Section 4 the development efforts, and Section 5 the laboratory calibration and wind tunnel testing efforts.

During this program three Model S and three Model E Maxometers were fabricated, calibrated and delivered. The three Model S units and one of the Model E units were used in the NASA-Langley wind tunnel tests.

NOTE: The hardened steel rod (see Fig. 3-3) had to be replaced by a ceramic coated rod due to a rod corrosion problem from the salt air environment.

Section 2

MAXOMETER SPECIFICATIONS

2.1 GENERAL

The Maxometers, Model S, shall be capable of monitoring the peak winds in the vicinity of space vehicle launch towers and surrounding terrain. Winds to be measured include the induced flow from space vehicle launch and wind conditions caused by natural phenomena such as storms, hurricanes, etc. The Maxometer shall be capable of measuring the peak-induced winds during the launch phase and maintaining a recording of this reading after the instrument has been exposed to the rocket engine exhaust environment after launch. The Maxometer shall be reusable with a minimum of refurbishment.

2.2 WIND SPEED RANGE

Total Range: 8 - 200 m/sec

This may be divided into two ranges as follows:

Low Range:	8 - 80 m/sec	at temperature = 60°F (15.6°C) pressure = 14.7 psia (1013 mb)
High Range:	20 - 200 m/sec	at temperature = 1000°F (538°C) pressure = 14.7 psia (1013 mb)
Maximum Dynamic pressure:	$\simeq$ 200 lb/ft^2	at 1000°F (538°C), 14.7 psia (1013 mb)
Minimum Dynamic Pressure:	$\simeq$ 1.0 lb/ft^2 (4.88 kg/m^2)	at 60°F (15.6°C), 14.7 psia (1013 mb)

2.3 ACCURACY

Design Goal: $\pm$ 5% of true reading

Ambient temperature and pressure data are assumed to be available for density correction factors to meet this accuracy requirement. Therefore, this accuracy shall apply to the velocity as determined from a dynamic pressure measurement.

2.4 RESPONSE

The Maxometer shall be designed to maintain the ±5% accuracy for the respective ranges under the following conditions.

Low Range (8 - 80 m/sec)

25 m/sec	linear velocity change in 2.0 sec in natural environment

High Range (20 - 200 m/sec)

130 m/sec	velocity change in 0.25 sec in natural environment
200 m/sec	velocity change in 0.25 sec in the launch environment (1000° - 2000°F temperature) (538° - 1093°C)

The weathervaning response of the Model E Maxometer shall be sufficient to align the instrument along the velocity vector with sufficient accuracy to meet the ±5% dynamic pressure accuracy requirements (Section 2.3) when measuring the 130 m/sec velocity change in 0.25 sec (natural environment).

2.5 ENVIRONMENT

2.5.1 Temperature

Natural Environment:	20° - 120°F (-6.7° to 48.9°C)
Launch Environment: (Model S only)	Temperature at 20 - 40 meters from exhaust flame. Temperatures in the 1000° - 2000° F (538° - 1093°C) range for 10 sec are anticipated.

2.5.2 Vibration (Acoustic and Otherwise)

The vibration and acoustic criteria will be consistent with the Saturn launch complex environment.

2.5.3. Other

The Maxometer is expected to operate for extended periods without degradation in the high humidity and salt water atmosphere at the Kennedy Space Center launch site.

2.6 ACCESSIBILITY

The readout device shall be readily accessible for periodic readings.

2.7 DESIGN RESTRICTIONS

The method of monitoring the peak wind speed shall not require electrical means nor consist of rubbing surfaces which may generate static electricity.

2.8 WIND DIRECTION

For the Model S Maxometer, orthogonal units will be deployed and wind direction resolved, assuming that the peak wind occurs simultaneously for each unit. The Model E Maxometer will not attempt to discern wind direction, but will record the maximum peak wind regardless of direction by weather-vaning into the wind.

Section 3
MAXOMETER DESIGN

3.1 GENERAL FEATURES

The Peak Wind Speed Anemometer or "Maxometer" was designed to meet the requirements and specifications of Section 2. The design process involved selection of a concept; evaluation of design parameters by computer simulation; design analyses of error sources, structure, materials, and Model E Weathervaning; and a study of performance tradeoffs. The following sections present the essentials of each one of these phases of Maxometer design. The resulting configurations, Models S and E, are shown in Figs. 3-1, 3-2 and 3-3. Figures 3-4, 3-5 and 3-6 show finished assemblies and details as tested in the wind tunnel tests described in Section 5. Also, some aspects of this design were the results of problems during the development phase (Section 4).

The Maxometer, Figs. 3-1 through 3-6, consists of a flat disk mounted on a rod. The rod is attached to a piston inside a cylinder. Inside the cylinder are two linear springs. The principle of operation is a force balance between the dynamic pressure force created by the wind on the disk and the spring compression force. A one-way ball clutch acting between the rod and cylinder end allows the disk-rod piston assembly to translate under wind loading but not return when this load is removed. After visual reading of a graduated scale on the cylinder of piston displacement, the Maxometer is reset by depressing the ball cage which disengages the balls and allows the disk to be returned by the compression springs. Also incorporated into the Model S version is a zero adjust mechanism to bias the weight of the moving parts (disk, rod, piston, etc.) when the unit's orientation is fixed at other than horizontal. Otherwise, the primary difference between the Model S and E configurations is that the Model S incorporates high temperature materials for the launch environment and has a fixed orientation. The Model E is designed for ordinary meteorological environment and is mounted such that

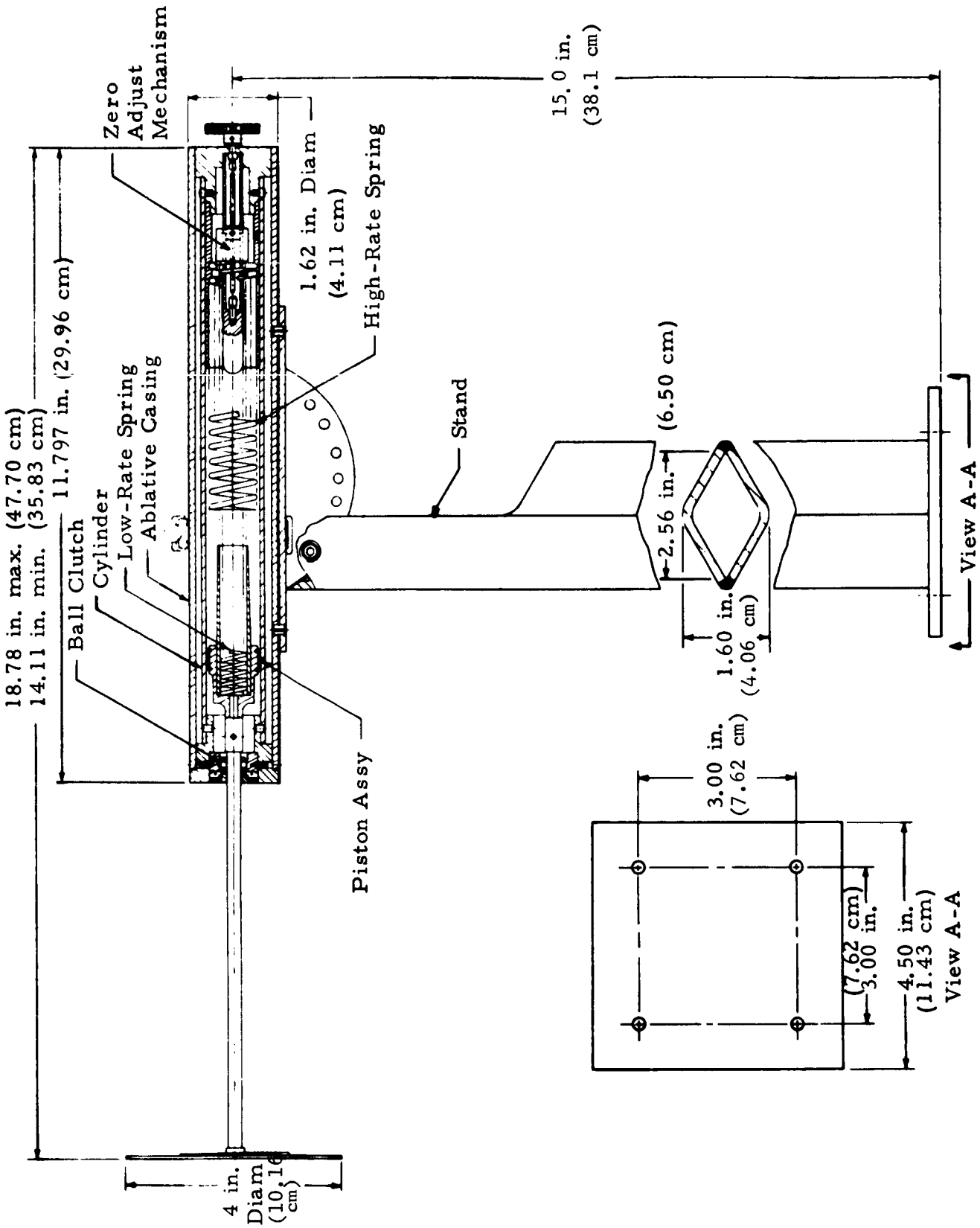

Fig. 3-1 - Maxometer Model S Configuration

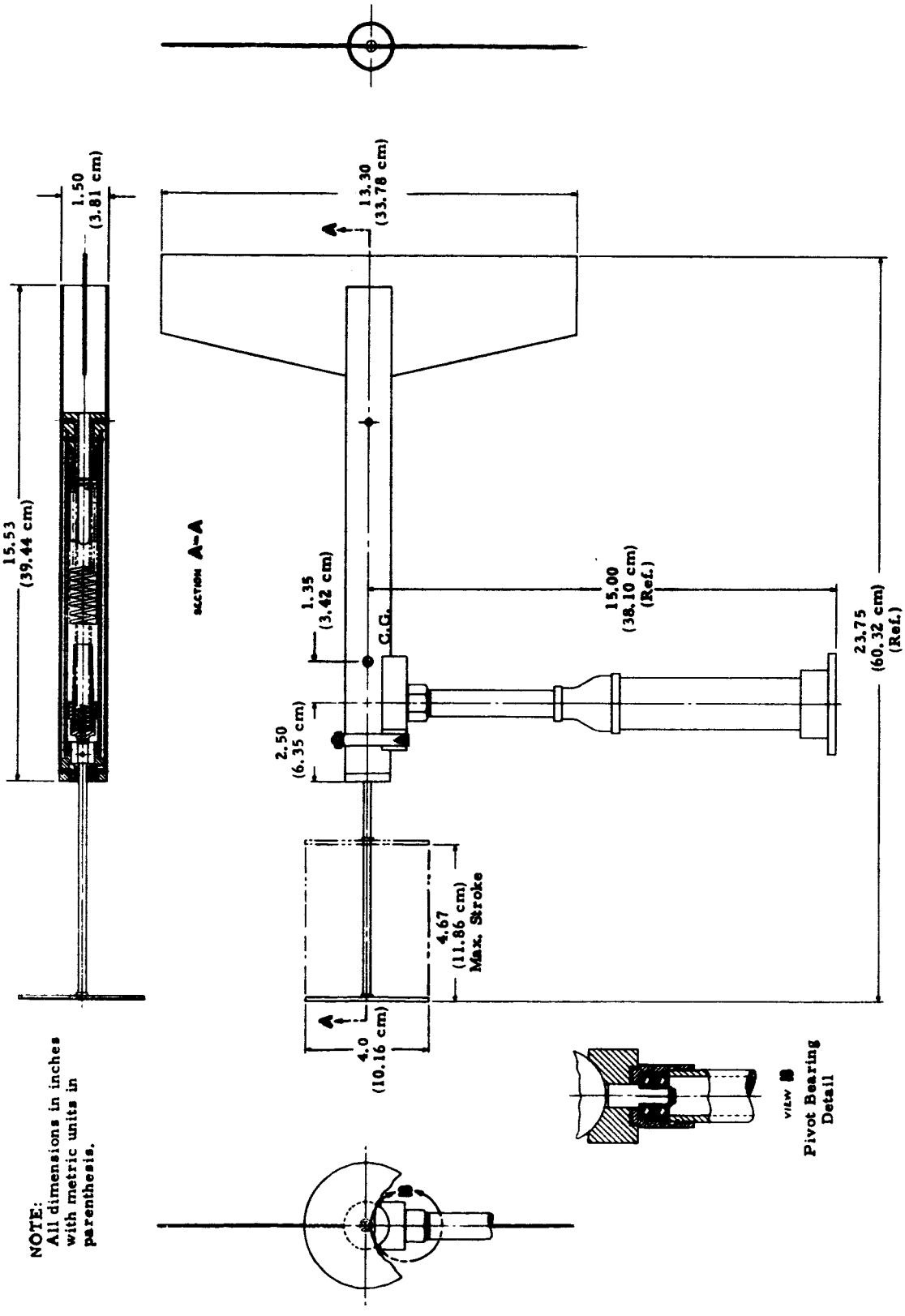

Fig. 3-2 - Maxometer Model E Configuration

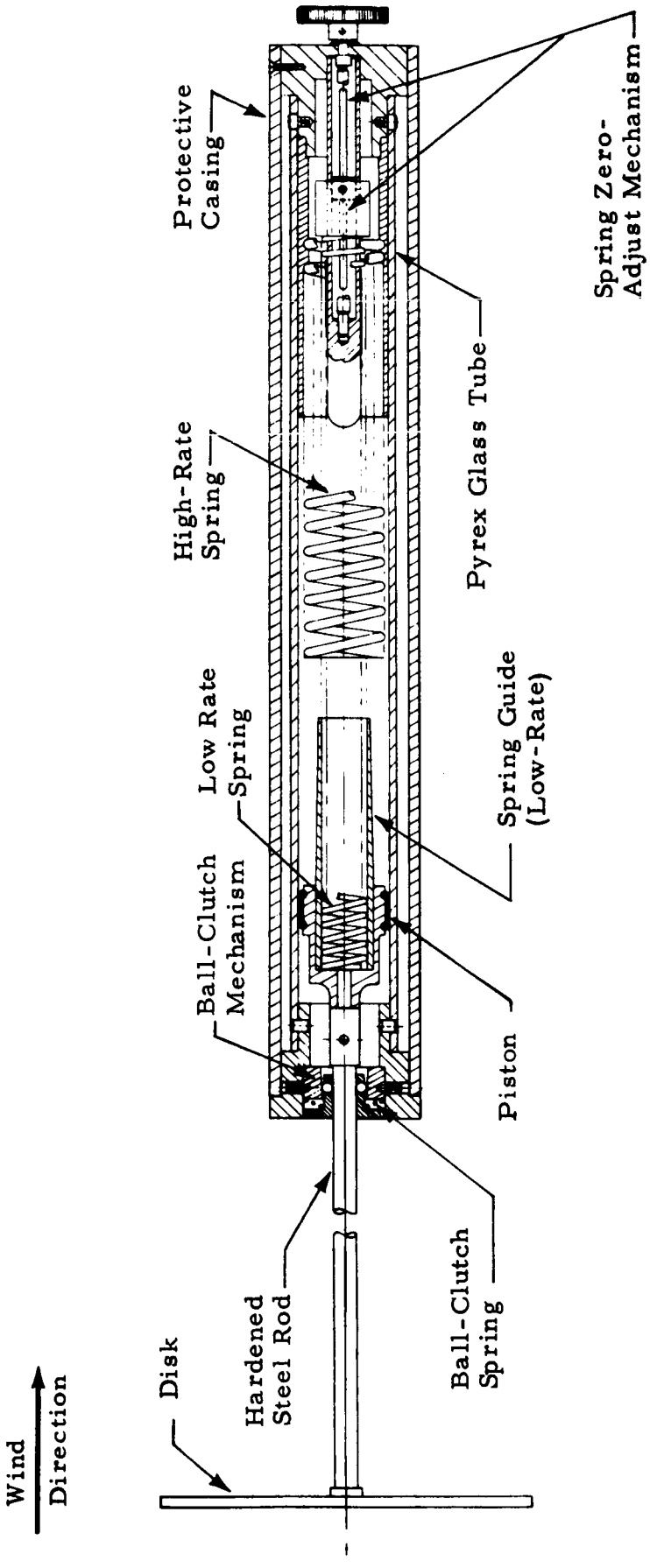

Fig. 3-3 - Maxometer Configuration Model S

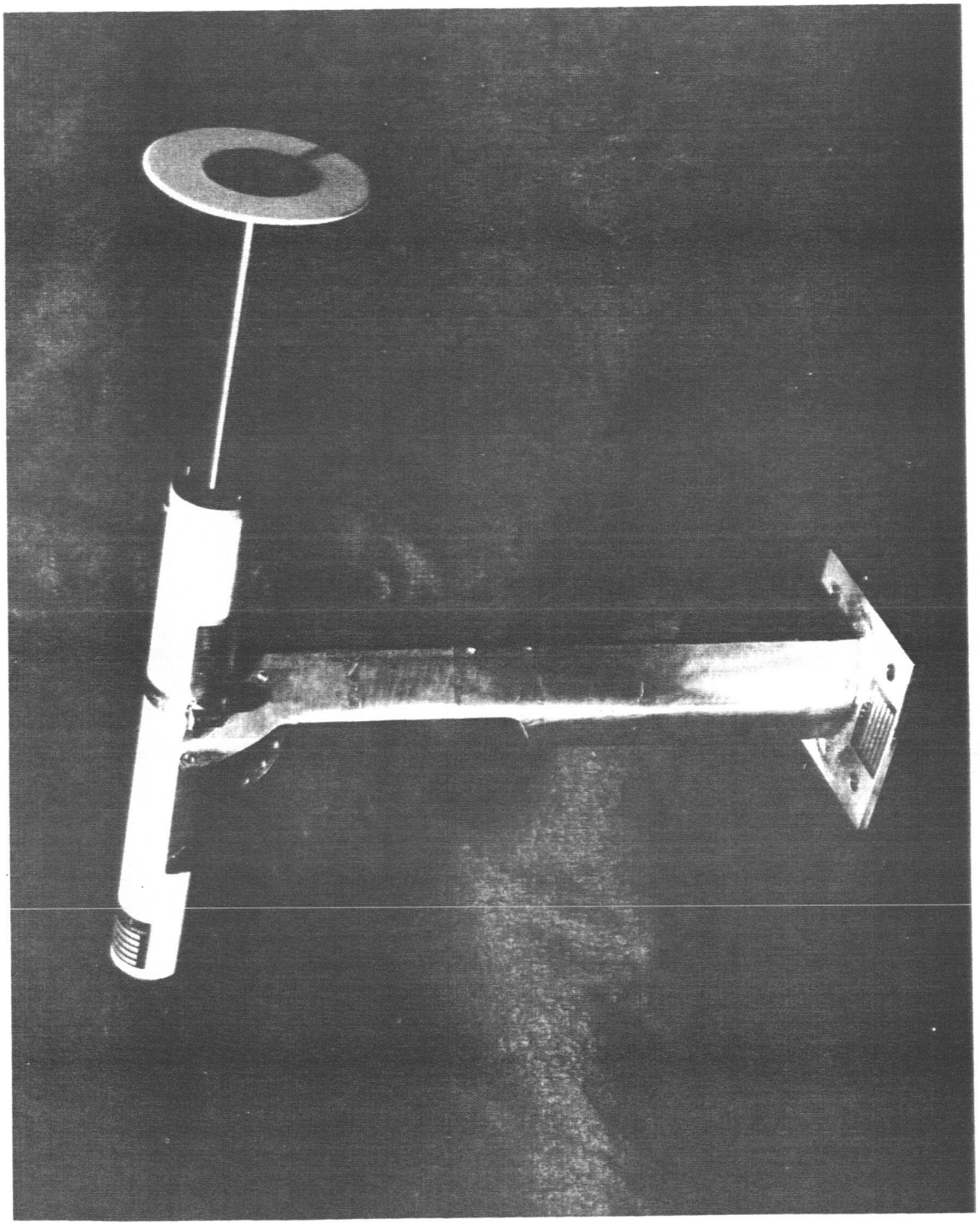

Fig. 3-4 - Model S Maxometer Assembly

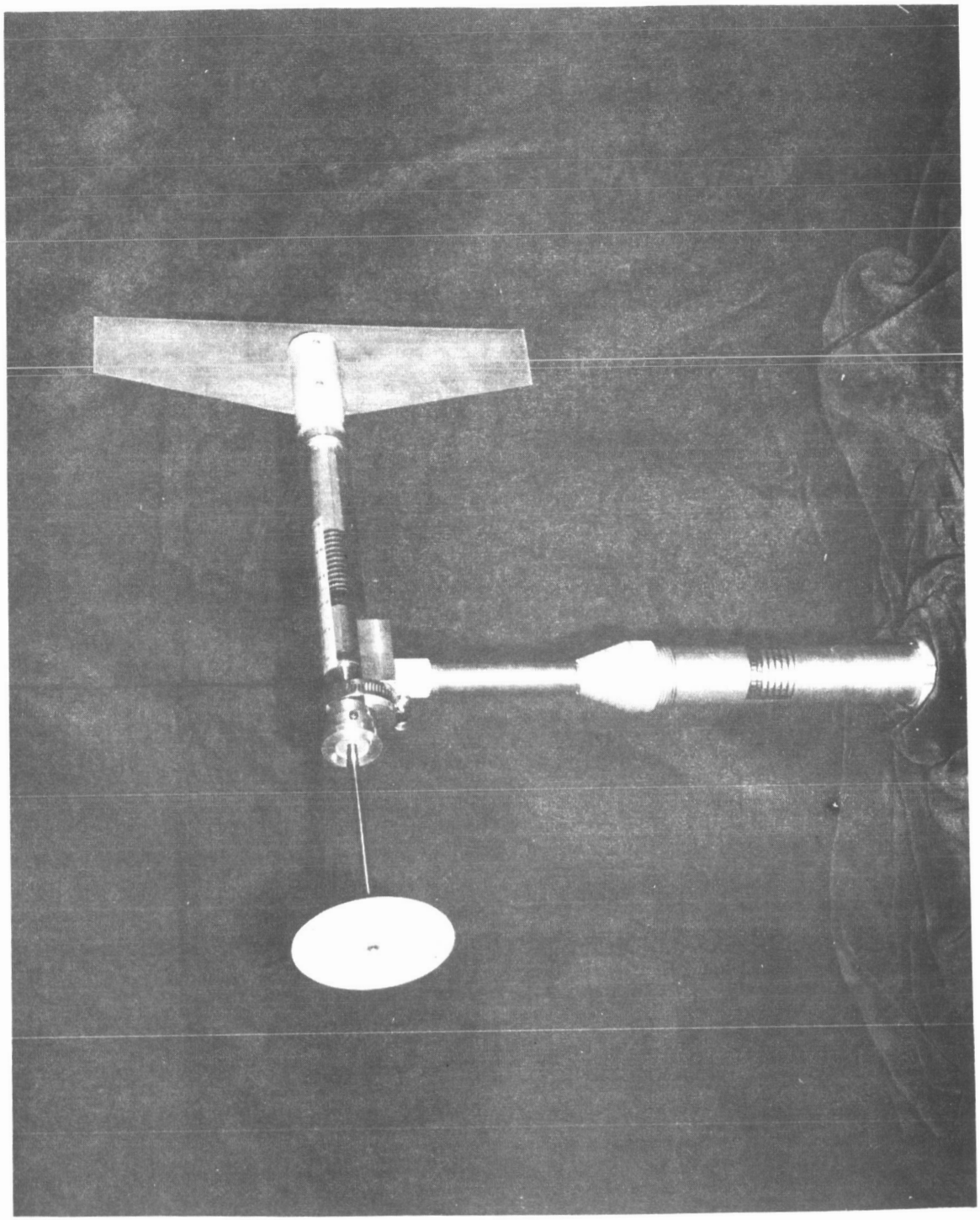

Fig. 3-5 - Model E Maxometer Assembly

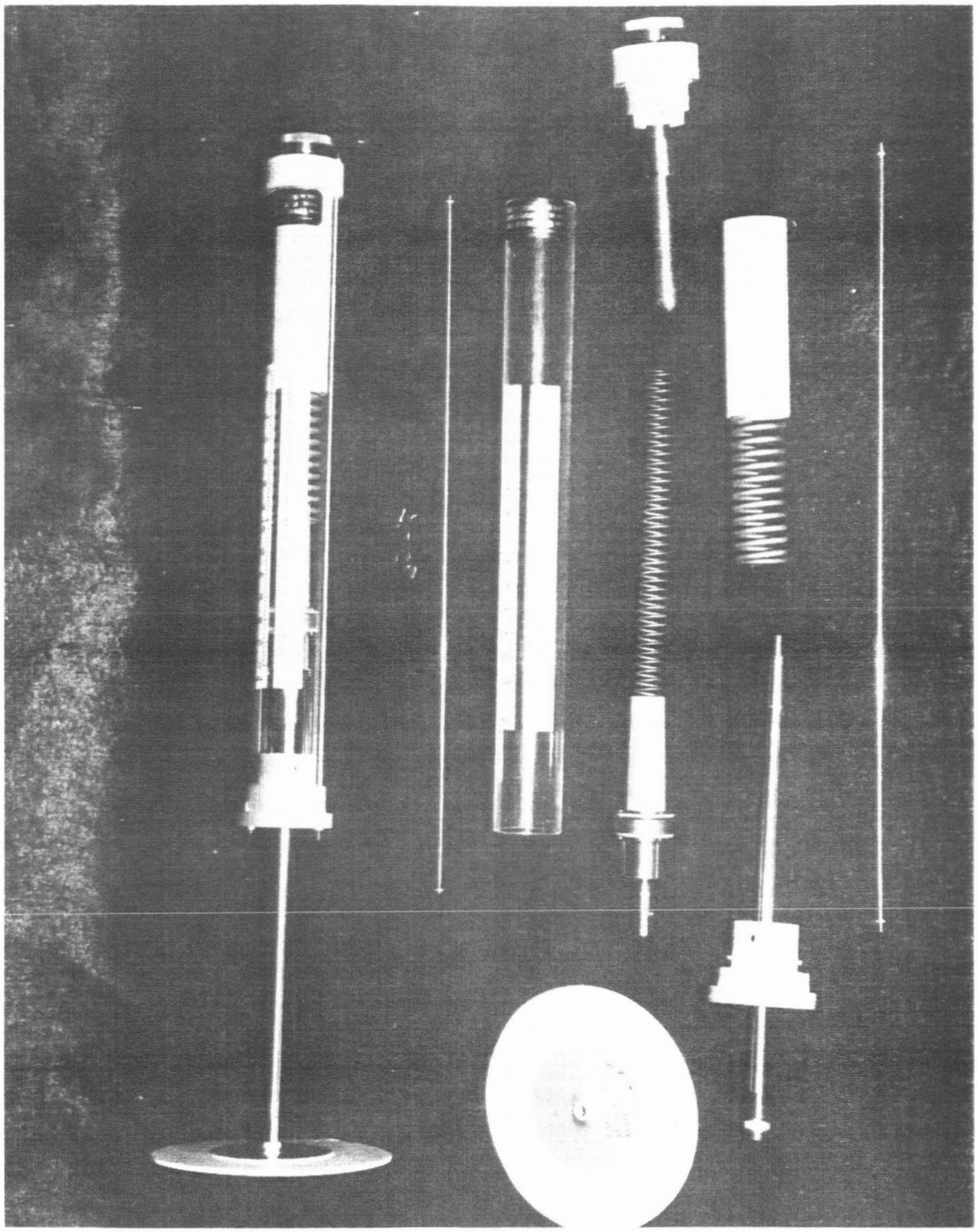

Fig. 3-6 - Maxometer Subassemblies (Model S)

the instrument is free to pivot in the horizontal plane (or "weathervane") for wind vector alignment.

3.2 CONCEPT

3.2.1 Sensing Method

Within the general field of anemometry, two devices which actually measure true wind speed accurately without disturbing the flow are: the laser velocimeter and the sonic anemometer. All other devices rely on aerodynamic drag and are therefore a means of measuring dynamic pressure, q. Wind velocity is related to q by the expression

$$V = \sqrt{\frac{2q}{\rho}} \quad . \tag{3.1}$$

Density, ρ, is a function of pressure and temperature for an ideal gas. The normal excursions of pressure, temperature and composition of air during usual atmospheric conditions can be figured into a correction factor, modifying ρ, to determine the correct wind velocity for a measured value of q. However, during environmental extremes such as the expected temperatures during Saturn launch ($1000^{\circ}F$ or $538^{\circ}C$) coupled with the unknown gas composition, the density can only be approximated. The same condition is true to a lesser extent during material environmental extremes incurred during violent storm activities. Wind velocity cannot be accurately calculated from q under these conditions. The measurement of q is accurate, however, and is not compromised by these factors.

3.2.2 Direct Drag Concept

The basic concept used in direct drag devices is that of measured pressure drag on a known body held normal to the air stream. The direct drag device is a force measurement instrument in which $q = F/AC_d$ for a known reference area, A, and a known (calibrated) drag coefficient C_d.

The chosen drag body for the Maxometer is a simple flat disk, since the C_d is almost a constant value through the expected Reynolds number (Re) range. Hoerner (Ref. 1) indicates a constant C_d value of 1.17 for Re values above 10^4. The Maxometer drag device is a flat disk mounted on a rod. The rod is attached to a piston inside a cylinder. Inside the cylinder are two linear springs (Fig. 3-3). The principle of operation is a force balance between the dynamic pressure force created by the wind on the disk and the spring compression force. A one-way ball clutch, acting between the rod and cylinder end, allows the disk and piston to translate under wind loading but not return when this load is removed. Resetting the Maxometer is accomplished by depressing the ball cage, which disengages the balls and allows the disk and rod to be returned by the compression springs. Readout for the Maxometer is a direct visual reading of a graduated scale on the cylinder, which yields dynamic pressure, q. As discussed earlier, the velocity is then related as indicated in Eq. (3.1).

3.3 COMPUTER SIMULATION

An analog mathematical model was produced so that sizing of the various components could be determined from its performance characteristics under wind response inputs. The initial program had a nonlinear spring force input to make the wind velocity directly proportional to spring displacement. This was later changed for reasons as discussed in Section 4.1, with the spring force subsequently changed as indicated on the following page. The free body diagram and system equation are as follows. Terms are further defined in the Nomenclature.

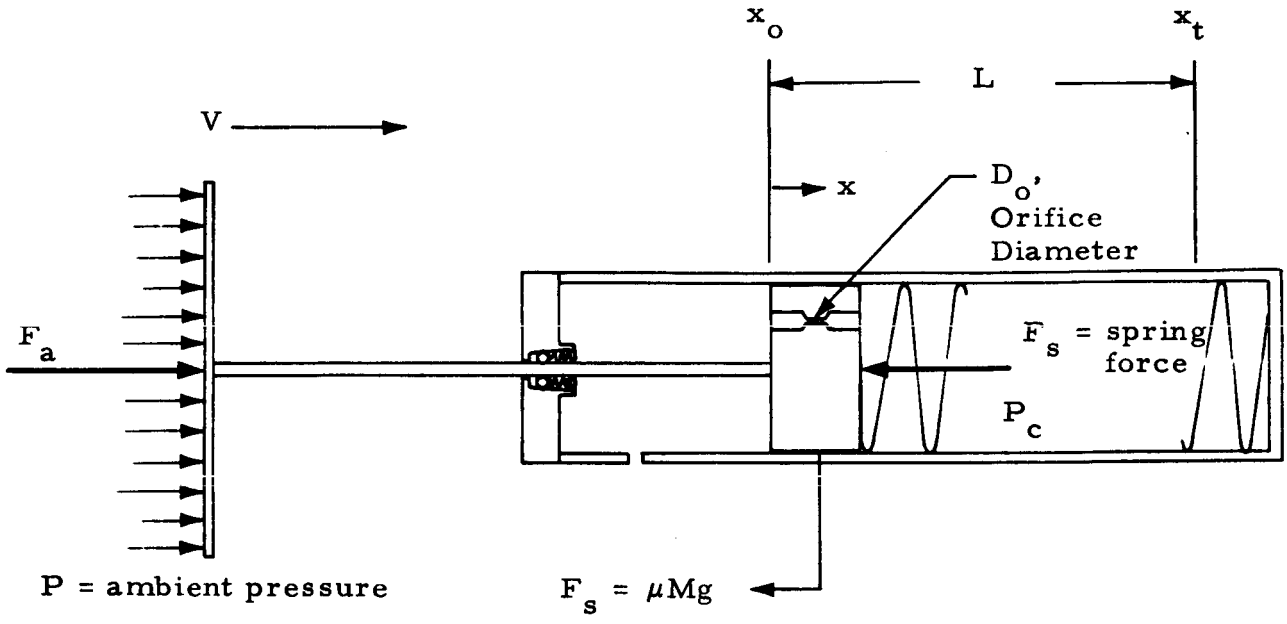

For a nonlinear spring the system equation is:

$$M\ddot{x} - \left[\frac{C_d P}{2gRT} A_d - C_o \frac{\rho}{2} A_p \left(\frac{D_p}{D_o}\right)^4\right]\dot{x}^2 + \frac{C_d P}{gRT} A_d V\dot{x} + ax^2 = \frac{C_d P}{2gRT} A_d V^2 - \mu Mg \qquad (3.2)$$

and for a linear spring system the ax^2 becomes a Kx term.

The terms that were considered independent variables and received parametric variation were: disk area (A_d), piston size (D_p), orifice size (D_o) and piston total displacement (L). The remaining terms are dependent variables and were put into the computer program after they had been calculated in view of their respective boundary conditions. The program output records the following parameters: wind velocity (V), piston displacement (x), piston velocity ($\dot{x}$), piston acceleration ($\ddot{x}$) and spring force (F_s) as a function of time.

A means of inserting friction into the program presented a problem. As programmed, friction was input as a dominant accelerating force, with a SIGN opposing the piston (or disk) velocity vector. This characteristic caused erroneous results at low wind speeds and when the disk velocity passed through zero. Friction was finally deleted because of overly complex simulation logic and the effects on system dynamic performance were found to be very minor.

The original computer simulation runs were made using a nonlinear spring system. Figures 3-7 and 3-8 are example computer runs for the nonlinear system and launch wind condition; i.e., wind input of 200 m/sec in 0.2 seconds. These two figures are for identical conditions except for the amount of damping (size of orifice). Figure 3-7, which has the larger damping, shows that no overshoot in displacement exists which is the desired result. The change to a two-linear spring system, as shown in Fig. 3-3, yielded traces as shown in Fig. 3-9.

The result of the computer simulation study was to indicate that the amount of damping (orifice size) is sufficient to provide a minimum of overshoot or error for the Maxometer as fabricated. Final choice of piston displacement was not a direct result of this study due to accuracy considerations, as mentioned in Section 3.4. However, the disk diameter of 4.0 in., piston size of 1.0 in., and orifice diameter of 0.020 in. were a result of this study.

3.4 DESIGN ANALYSES

Independently of the computer simulation of the Maxometer, a number of areas were investigated to guide the design efforts. Some of these areas were related to instrument accuracy (resolution, acoustic pressure, rain, vibration, and wind vector alignment), while others were related to the velocity displacement characteristics and to structural and temperature considerations. These areas are discussed in the following paragraphs.

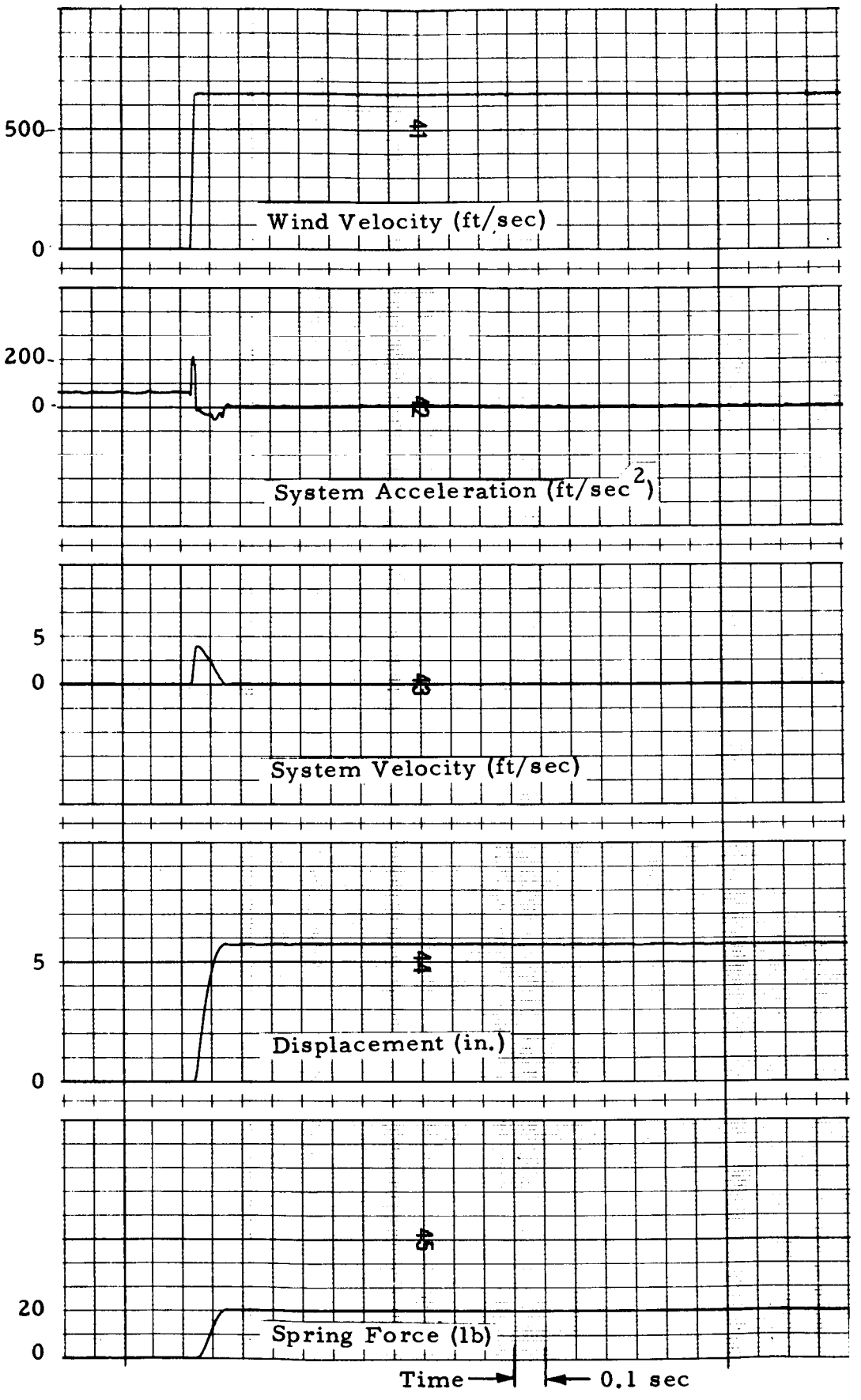

Fig. 3-7 - Analog Simulation of Mathematical Model for Nonlinear Spring System (Large Damping)

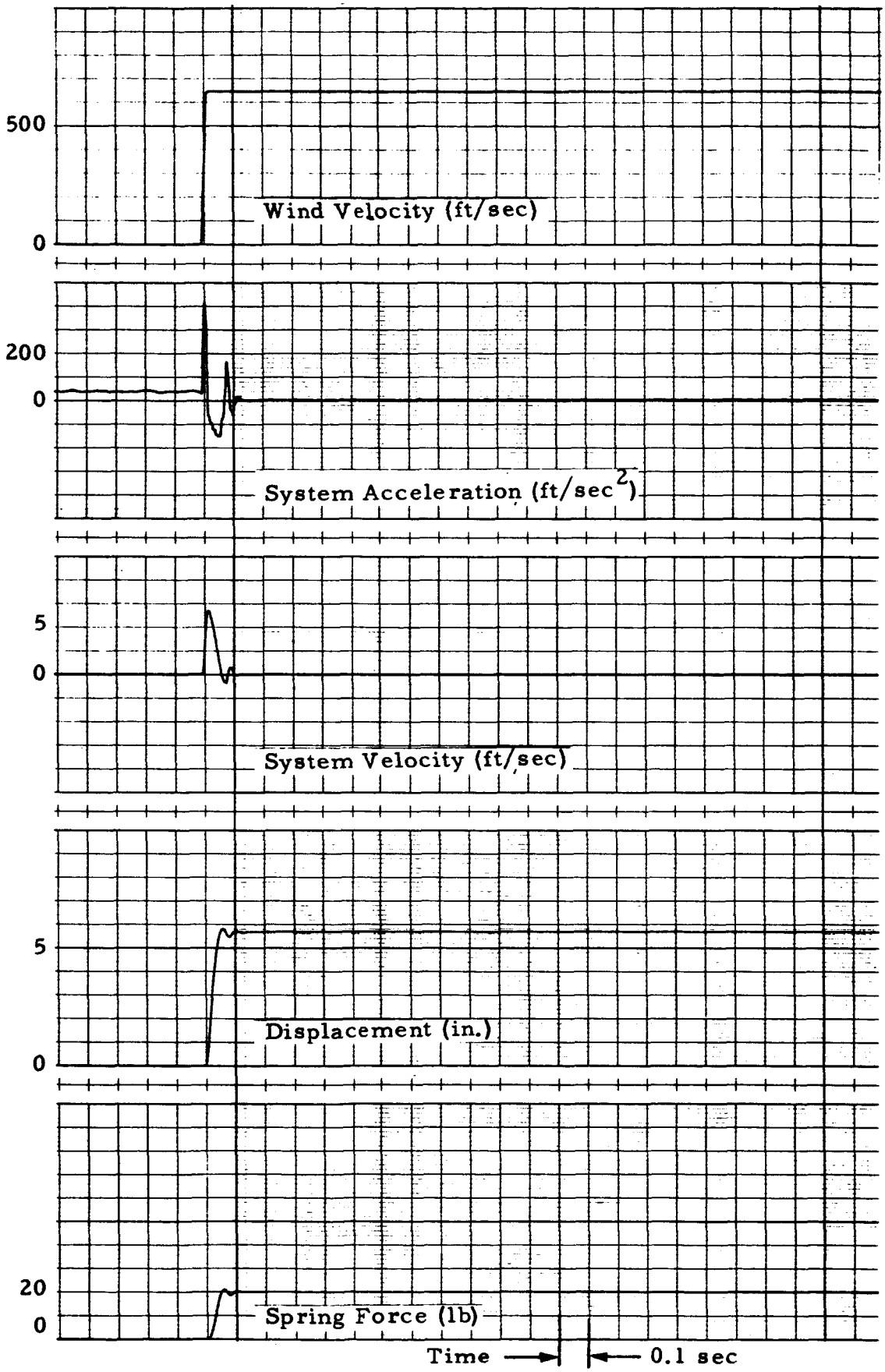

Fig. 3-8 - Analog Simulation of Mathematical Model for Nonlinear Spring System (Small Damping)

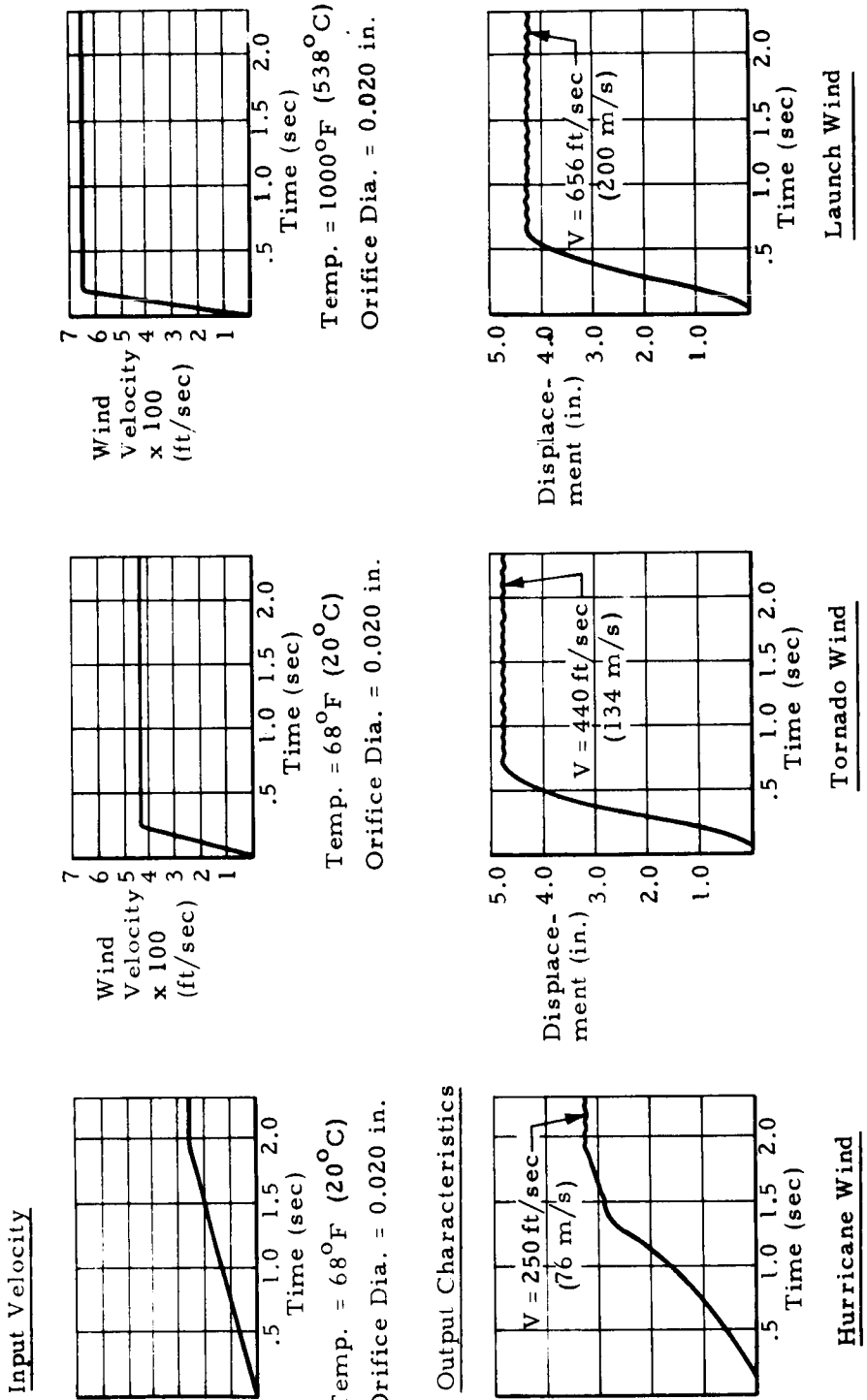

Fig. 3-9 - Maxometer Dynamic Performance Characteristics

3.4.1 Resolution Error

A Maxometer design goal accuracy of ±5% of reading (Section 2.3) will require a resolution capability somewhat better than this accuracy. This resolution is established by the "naked eye" scale resolution and the instrument spring rate. An expression for percent error was derived for a system using a linear spring ($F_s = Kx$) and one using a nonlinear spring ($F_s = ax^2$). For a linear two-spring system, as shown in Fig. 3-3,

$$F_s = \frac{1}{2} \rho C_d A_d V^2 = K_1 x + K_2 (x - x_1) \tag{3.3}$$

where

K_1 = low-rate spring constant, lb/ft

K_2 = high-rate spring constant, lb/ft
= 0 for $x \leq x_1$

x_1 = displacement to contact of the high rate spring

Differentiating the above equations, the velocity error dV/V for a given scale displacement resolution dx is

$$\frac{dV}{V} = 100 \frac{(K_1 + K_2)\, dx}{\rho C_d A_d V^2}, \quad \text{percent} \tag{3.4}$$

or

$$\frac{dV}{V} = \frac{100(K_1 + K_2)\, dx}{2\left[(K_1 + K_2)x - K_2 x_1\right]} \tag{3.5}$$

In a similar manner, the dynamic pressure error, dq/q, was derived.

$$\frac{dq}{q} = \frac{100(K_1 + K_2)\, dx}{C_d A_d q} \tag{3.6}$$

or

$$\frac{dq}{q} = \frac{100(K_1 + K_2)\, dx}{(K_1 + K_2)\, x - K_2 x_1} \tag{3.7}$$

Thus, it can be seen from Eqs. (3.5) and (3.7) that the velocity resolution error is 1/2 the dynamic pressure error.

Using Eq. (3.4), the resolution error for the Maxometer configuration in Fig. 3-3 was computed and is illustrated in Fig. 3-10. Velocity errors for scale resolution from 0.10 to 0.015 in. is shown. As the curve illustrates, the resolution error could be improved by increasing the velocity at which high rate spring contact is made. This is a recommended improvement for the instrument. This may be determined by using Eq. (3.5) and equating $x = x_1$. Thus,

$$x_1 = \frac{100(K_1 + K_2)\, dx}{2K_1 \frac{dV}{V}} \tag{3.8}$$

Substituting the appropriate spring rates, the value of x_1 for a velocity error of 3% (= low-rate spring error) and a dx resolution of 0.010 in. is $x_1 \simeq 3.5$ in. Alternatively, this error may be reduced by decreasing K_2.

The resolution characteristics of a Maxometer with a nonlinear spring ($F_s = ax^2$) were evaluated from the equation

$$\frac{dV}{V} = \frac{200\, ax\, dx}{\rho\, C_d\, A_d\, V^2} \tag{3.9}$$

A simplification of Eq. (3.4) yields the following relation for a single constant rate spring system.

$$\frac{dV}{V} = \frac{100\, K\, dx}{\rho\, C_d\, A_d\, V^2} \tag{3.10}$$

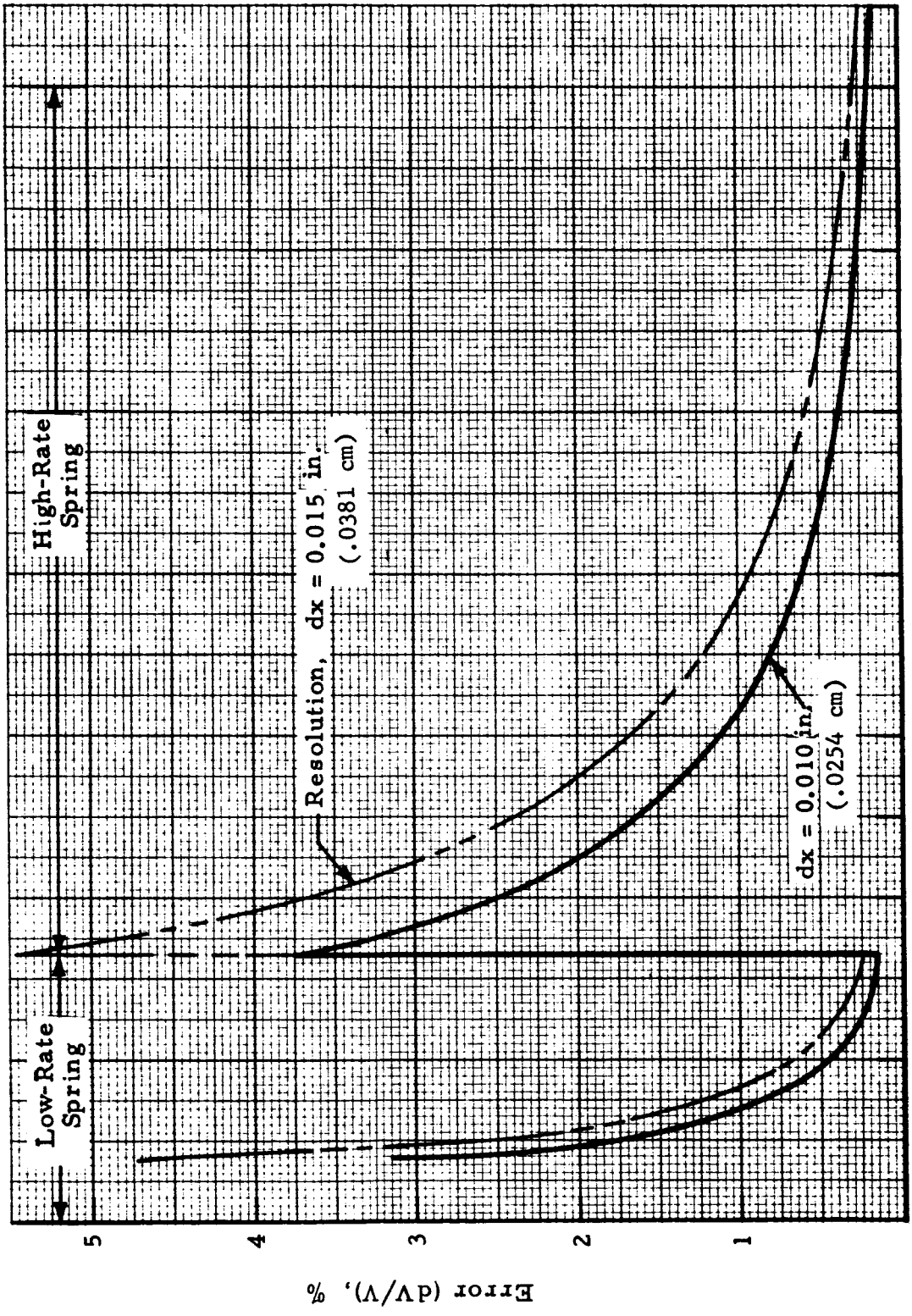

Fig. 3-10 - Maxometer Resolution Error

The constants a and K are determined from the maximum dynamic pressure (q_{max}) and the maximum total spring deflection (x_{max}). Substitution of equivalent values of these constants and combining Eqs. (3.9) and (3.10) yields velocity resolution error ratio (η) for comparing the nonlinear to the linear spring. Thus,

$$\eta = \frac{\left(\frac{dV}{V}\right)_{nonlinear}}{\left(\frac{dV}{V}\right)_{linear}} = \frac{2x}{x_{max}} \qquad (3.11)$$

From this relation, it can be seen that the nonlinear spring has superior error characteristics for x/x_{max} values less than 0.5. However, as the deflection approaches x_{max}, the error of the nonlinear spring is twice that of the linear spring. This, plus the excessive costs of a nonlinear spring, are the primary reasons for the two-linear spring design in Fig. 3-3.

3.4.2 Acoustic Pressure Force

The effects of acoustics on the peak wind anemometer were examined (Refs. 2 through 5). When wave-propagated energy falls on a reflecting surface, such as the Maxometer disk, it gives rise to a static pressure on that surface. The phenomenon is a universal property of wave motion and applied equally to acoustic waves and electromagnetic waves. In the case of sound waves, the static pressure on an area, A, is

$$P_s = 2E_s/c \ (\text{dynes/cm}^2) \qquad (3.12)$$

where E_s is the sound intensity (ergs/cm^2/sec), and c is the velocity (cm/sec). The force on the area A is

$$F = P_s A \ , \qquad (3.13)$$

assuming that the wave is incident normally on the surface.

At constant amplitude, the energy in a propagating sound wave is directly proportional to the square of the frequency (f^2), or inversely proportional to the square of the wave length ($1/\lambda^2$). The effective receiving area of an object, whose maximum dimension (a) is less than $\lambda/2$, is directly proportional to the square of the wavelength. That is

$$A_r = \frac{\lambda^2}{8} \left(0 < a < \frac{\lambda}{2}\right) \tag{3.14}$$

When the dimension of the object is larger than $\lambda/2$, the effective receiving area approaches the geometrical area, which in the case of a disk is πa^2. This accounts for the fact that a microphone, whose size is small compared to the wavelength of sound incident upon it, has essentially flat response throughout the audible range.

The force on a disk, therefore, will be very nearly

$$F = \pi P_s a^2/8 \tag{3.15}$$

independent of wavelength, throughout the frequency range of interest. Then, since the pressure is related to the sound power by the equation

$$P = 20 \log \left(\frac{P_s}{P_o}\right) dB \tag{3.16}$$

where P is the sound power measured in decibels above the reference sound pressure, i.e., 2×10^{-4} dynes/cm^2, or 2.9×10^{-9} lb/in^2, the force is

$$F = (\pi a^2/8) \times 10^{P/20} \times 2.9 \times 10^{-9} \tag{3.17}$$

Figure 3-11 shows the force on 3-in. and 4-in. diameter disks for various sound power levels. Launch data for the AS-503 (Ref. 6) indicate maximums of up to 160 dB, with the majority maximums at 140 dB which place the acoustic forces at small values, especially when it is considered

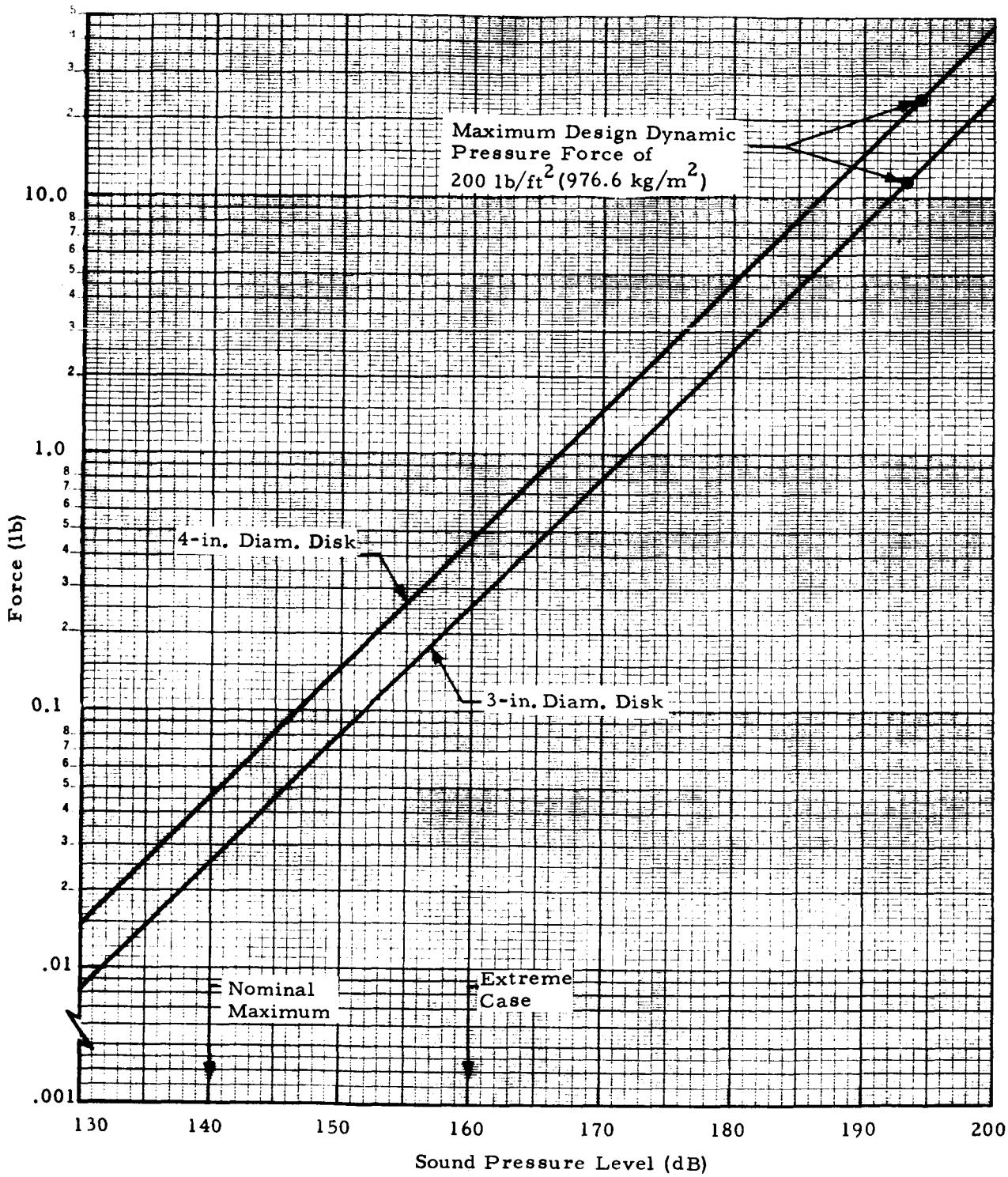

Fig. 3-11 - Acoustic Force in Critical Frequency Range (1300 to 6000 Hz)

that the high acoustic forces will be coincident with the measurement of high dynamic pressures.

3.4.3 Steady State Performance

As previously stated, the Maxometer operates on the basis of a force balance between the wind and spring forces. The basic steady state relationship is

$$q\, C_d\, A_d = K_1 x + K_2 (x - x_1)$$

or the dynamic pressure,

$$q = \frac{(K_1 + K_2)x - K_2 x_1}{C_d A_d} \tag{3.18}$$

where

K_1 = low range spring constant
= 0.468 lb/in. (design)

K_2 = high range spring constant
= 9.720 lb/in. (design) for $x_1 > 2.500$
= 0 for $x_1 < 2.500$

x_1 = low range displacement to high range spring contact
= 2.500 in. (63.5 mm)

C_d = disk drag coefficient
= 1.17 (design)

A_d = disk frontal area
= 0.0872 ft^2

Substituting these values into the above equation yields the following design performance relationships for the low and high ranges. See Fig. 3-12.

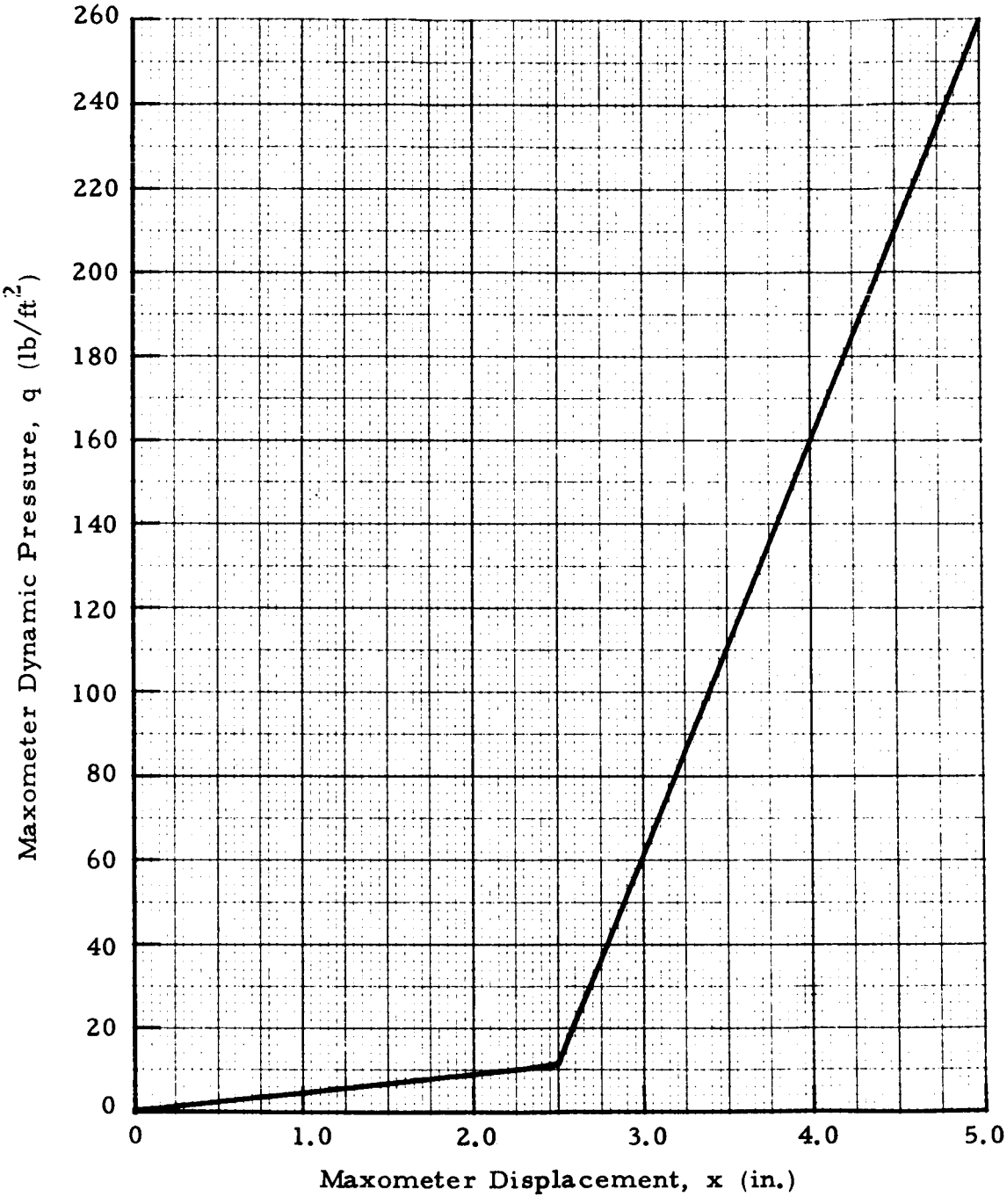

Fig. 3-12 - Maxometer Dynamic Pressure vs Displacement

Low Range

$$q = 4.59x \quad \text{lb/ft}^2$$

High Range

$$q = 99.88x - 238, \quad \text{lb/ft}^2 \qquad (3.19)$$

The wind velocity (V) is related to q by

$$V = \sqrt{\frac{2q}{\rho}}$$

or (3.20)

$$V = \sqrt{\frac{2RTq}{P}}$$

Substituting this in Eq. (3.18) yields the relation for velocity vs displacement (x), or

$$V = \sqrt{\frac{2RT}{P\,C_d A_d}\left[(K_1 + K_2)x - K_2 x_1\right]} \qquad (3.21)$$

where

P = ambient pressure
= 2116 lb/ft^2 (1013 mb) at sea level, standard day

R = air gas constant
= 1716 ft^2/sec^2-$^\circ$R

T = temperature, $^\circ$R
= 520°R (289°K) for standard day

Substitution of these values yields the following relations for velocity versus displacement as illustrated in Fig. 3-13.

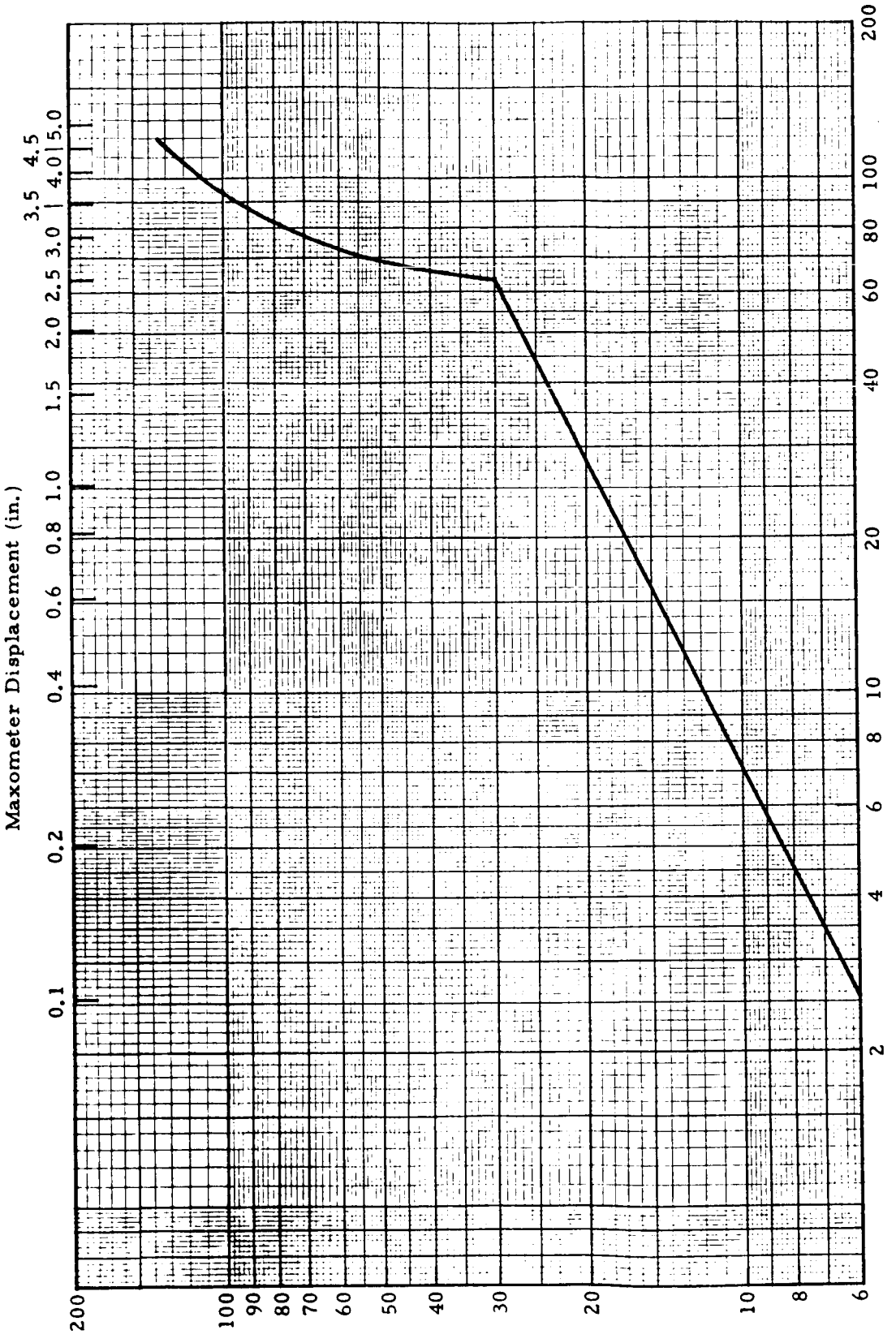

Fig. 3-13 - Maxometer Velocity vs Displacement Characteristics

Low Range

$$V = 62.2\sqrt{x}\ , \qquad \text{ft/sec}$$

High Range

$$V = 290.2\sqrt{x - 2.383}\ , \qquad \text{ft/sec} \tag{3.22}$$

where

x = displacement, in.

In metric terms these relations are

Low Range

$$V = 3.762\sqrt{x}\ , \qquad \text{m/sec}$$

High Range

$$V = 17.55\sqrt{x - 60.53}\ , \qquad \text{m/sec} \tag{3.23}$$

where

x = displacement, mm

3.4.4 Temperature Effects

A thermal expansion analysis of various components was performed because of the large temperature variation (ambient to 1000°F). The technique used was to determine the size increase due to temperature, compare this to the mating part, and then compute the resulting increase in stress due to interference should interference exist. An increase in temperature from ambient to 200°F was used inside the silicon glass ablative cover and to 1000°F outside the cover. The expansion was computed by using the materials' coefficient of linear expansion times the initial size and respective temperature differential. Primary components of concern were the mating rod and

cylindrical components making up the disk rod, ball clutch, piston, and glass cylinder as shown in Fig. 3-3. Expansion in the radial and axial directions were considered. Tolerances and clearances of functioning parts were set to allow freedom of motion during maximum temperature extremes, and maintain a given piston displacement after exposure (such as after launch soak). No particular problems were indicated as a result of this design analysis.

Temperature effects on the spring rate characteristics were a particular concern in the selection of a spring material. Ni-Span-C was found to have essentially a constant shear modulus of elasticity over the temperature range of 0-200^{o}F and was selected.

3.4.5 Vibration

Because the Maxometer is a spring-mass system with its own resonant frequency, it was necessary to investigate the vibration of both the Maxometer stand and the Launch Umbilical Tower (LUT) mounting. Data contained in Ref. 6 were examined for detrimental frequencies during Saturn V launch operations and for possible mounting points. The term detrimental frequencies is used to denote those frequencies with large power plot peaks at or near the Maxometer or stand frequencies. Calculated natural frequencies of the stand are 96 Hz and 19 Hz for a frontal and side vibrational mode, respectively. The natural frequencies of the Maxometer are 3 and 15 Hz, depending upon which spring is being compressed (the 3 Hz frequency for the low rate spring and 15 Hz for the high rate spring). As was anticipated, no station on the LUT is free of vibration. Certain portions and stations do appear better than others in that both the peak amplitude, root-mean-square amplitude, and power spectral density are small at the critical Maxometer frequencies. The most promising mounting positions would be on the main columns which have maximum peak loads of 0.8 g, with an rms value of 0.6 g at low frequencies, 1 to 2$\frac{1}{2}$ Hz. Secondary to these would be the horizontal box sections where the peak loading is 8 to 9 g, rms loading around 5 g's and frequencies around 180 Hz. At best then, no position is perfect and

care should be exercised to see that a low amplitude and force location is chosen for the Maxometer mounting.

3.4.6 Structural Analysis

During the design of any new system, a portion of the work is directed toward determining the loads and their resulting stresses. Generally, certain items in the design can be neglected from any stress analysis because it is determined by inspection that they either have very small loadings or have very large sections for the load to be carried. Those items possessing neither of these criteria require stress analysis. For the Maxometer, three major items required more than just a cursory examination. These were the ball-clutch mechanism, the stand, and the rods holding the ends together.

3.4.6.1 Ball-Clutch Mechanism

The loading on the balls in the clutch mechanism were examined because of the point loading effect. The free body diagram is shown below.

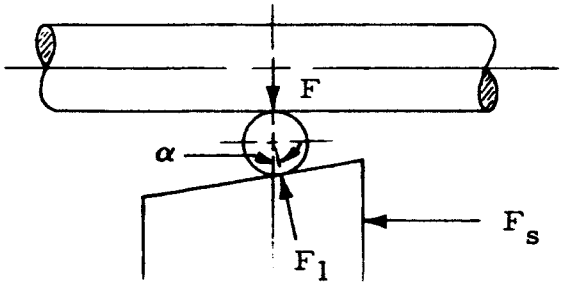

The load per ball is:

$$F_1 = \frac{F_s/n}{\sin\alpha} = \frac{25/6}{0.04362} = 95.5 \text{ lb} \qquad (3.24)$$

where

n = number of balls

Since there are no stress equations applicable to the ball-clutch configuration, the stresses were calculated for boundary conditions which were considered worse than, and better than, the existing conditions. From this information, it would become apparent if the ball stress would cause fracture. The stress (compressive) equation and diagram for a sphere on a flat plate are (Ref. 7);

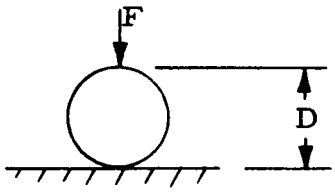

$$S_c = 0.918 \sqrt[3]{\frac{F}{D^2\left[\frac{1-\nu_1^2}{E_1} + \frac{1-\nu_2^2}{E_2}\right]^2}} \qquad (3.25)$$

and for the sphere in a spherical pocket;

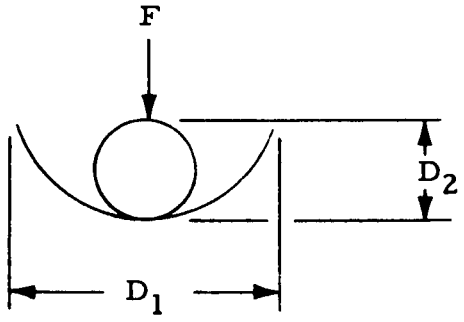

$$S_c = 0.918 \sqrt[3]{\frac{F\left(\frac{D_1 - D_2}{D_1 D_2}\right)}{\left[\frac{1 - \nu_1^2}{F_1} + \frac{1 - \nu_2^2}{F_2}\right]^2}} \qquad (3.26)$$

The stress obtained by substituting Poisson's ratio (ν), modulus of elasticity (E), and respective diameters for the two boundary conditions varies from 0.95×10^6 to 1.5×10^6 psi, and would appear to cause fracture. However, because of the facts that the stress is highly localized and triaxial, the calculated stress intensity can be somewhat higher than the material ultimate without producing serious damage. Experiments discussed in Ref. 7 verify this. The worst condition anticipated was highly localized dimpling of the rod surface at maximum rod displacement. This was minimized by using the largest size and number of balls feasible for the configuration.

3.4.6.2 Stand

The stand loading was approached from a cantilever beam having two concentrated loads, namely the Maxometer and stand. Assuming the maximum dynamic pressure of 200 lb/ft^2 acting on the frontal area, the Maxometer loading was calculated to be 25 lb and the stand approximately 6 lb. These two loadings produced a calculated stress of only 2000 psi maximum. This level stress is well below the limit for 316 stainless steel.

Another area on the stand that was examined is the roll pins holding the cradle to the stand. These two pins are under shear loading equal to the maximum wind loading. Manufacturers' recommended maximum loading for these pins is 4400 lb. The 25-lb Maxometer load is well below this value.

3.4.6.3 Rods

The two small rods which hold the Maxometer ends together were examined to ensure they could hold the Maxometer together under maximum load conditions. Maximum loading for the rods is when the disk-piston is displaced its full stroke (springs are fully compressed), as shown below.

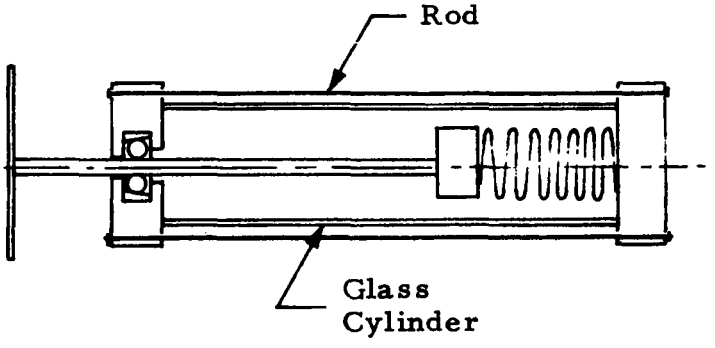

The rod stress is:

$$S = \frac{F}{A} = \frac{25/2}{\frac{\pi\left(\frac{1}{16}\right)^2}{4}} = 4075 \text{ psi}$$

For 0-80 threads the stress area is 0.0026 in^2. This value for area gives a stress of 4820 psi, which is very low and allows for a safety factor of 20. The rod tensile strength is approximately 80,000 psi.

3.4.7 Weathervaning Characteristics

The Model E Maxometer is designed to provide a measurement of peak wind velocities regardless of wind direction relative to the instrument. A tail fin is used to orient the freely pivoted unit into the wind and to damp any oscillation tendency. See Fig. 3-2. Response of the system is based on the damping ratio of the unit.

The criteria for selection of the damping ratio are a balance of amplitude or overshoot, time response, and the frequency ratio. Time response characteristic is most important because the unit must be oriented into the wind in less time than the expected maximum gust rise time.

A review of existing directional anemometer devices revealed that the most common damping ratio is approximately 0.6. This value was used as a design goal. However, MacCready and Rex (Ref. 8) report that an optimum damping ratio of 0.43 is desired, so that vane overshoot at intermediate frequencies compensates for attenuation at higher frequencies.

In determining the fin configuration required to provide a specific damping ratio, the optimum values of inertia, moment arm, fin area, and aspect ratio must be used. The following equations relate physical characteristics to damping ratio and wavelength:

$$\delta_r = \frac{2\pi \ell}{\lambda_N} \tag{3.27}$$

$$\lambda_N = 73 \left[\frac{I\left(1 + \frac{2}{AR}\right)}{\ell S} \right]^{1/2} \tag{3.28}$$

where

δ_r = damping ratio

λ_N = wavelength

I = inertia (0.0129 - 0.0146 lb-ft-sec^2)

ℓ = moment arm (1.0 ft)

S_f = fin area (0.22 ft^2)

$AR = b^2/S$ = aspect ratio

From Eq. (3.28) the span (b) can be found:

$$b^2 = \frac{2S}{\left[\left(\frac{\lambda_N}{73}\right)^2 \frac{\ell S}{I} - 1\right]} \qquad (3.29)$$

The inertia of the system varies due to the change in position of the piston-rod-disk combination at different wind velocities. The inertia change causes the damping ratio to vary slightly. Then:

$$\lambda_N = 21.8 \text{ ft/cycle } (6.64 \text{ m/cycle})$$

$$\delta_r = 0.257 - 0.299$$

$$b = 1.11 \text{ ft } (.338 \text{ m})$$

The above damping ratio is less than the target value of 0.6. Analysis of wind tunnel data (Section 5.2.4) revealed discrepancies in the theoretical determination of fin size. Errors in Ref. 8 consisted of deletion of factor of 2 in Eq. (3.27) and deletion of radical in Eq. (3.28). The erroneous form of these equations were used in the original design. Due to the errors, the initial calculations gave a wavelength $\lambda_N = 5.24$ for a damping ratio of $\delta_r = 0.59$.

The natural frequency of the system, due to aerodynamic loading at maximum dynamic pressure, is:

$$\omega_N = \frac{V_{max}}{\lambda_N} = 21.0 \text{ Hz}$$

V_{max} = maximum freestream velocity (458 ft/sec) at standard temperature and pressure

3.4.8 Rain

Since most extreme environmental phenomena are associated with some sort of precipitation, the effects of blowing rain were examined. An expression was derived for the force generated by the rain from the momentum equation. The derivation is as follows:

$$F = \dot{M}V = (\text{disk area})(\text{rainfall rate})(\text{rain weight})(\text{terminal velocity})$$

$$F = \frac{\left(\frac{\pi d^2}{4}\right)\left(r \times \frac{1}{60}\right)\left(\frac{62.4}{1728}\right)\left(V\right)}{386} = 11.8 \times 10^{-4}\, r\, V \qquad (3.30)$$

where r is the rainfall rate in inches per minute and V is the raindrop terminal velocity in inches per second. Using the rainfall rate (0.5 in./min.), terminal velocity (8.8 m/sec), and peak winds (30 m/sec) for the Gulf Transportation, Panama Canal and New Orleans (Ref. 9), the following forces were calculated. It was assumed that the wind component and rainfall component directions can be resolved into a resultant direction acting perpendicular to the drag disk. The calculated rain force was 0.0034 lb, and the wind rain force was 0.0119 lb, with a resultant force of 0.0121 lb. For the 30-m/sec peak wind, this resultant force represents an error of 1.21% of the wind force ($F = q A C_d = 0.99$ lb). Looking at the most critical point, which is the low extremity of the 8 to 200 m/sec design range, the resultant force represents 4% of the force required to displace the Maxometer.

It is to be noted that the rainfall rate used is an extreme amount, 1/2 in./min. For Huntsville, Eastern Test Range, Western Test Range, Sacramento, Wallops Test Range, and White Sands Missile Range, this rainfall rate is reduced by 40% or 0.3 in./min. Between this value and the estimates made in the preceding paragraph, the rainfall is seen not to be a significant contributor to Maxometer performance error.

3.5 MATERIALS

Each component of the Maxometer was selected in view of the particular environment and stress levels it would encounter. Two important factors were the high temperature and salt air. To protect the Maxometer against the 1000°F temperatures, a silicon glass ablative outer casing and end closures are utilized. In addition, the disk is a silicon glass laminate for high temperature and low weight. All other materials are either a stainless steel or a synthetic (e.g., Rulon), except for the springs. Particular attention was given to selection of the force balance springs. These are made of Ni-span-C, which has a constant coefficient of thermal expansion from ambient up to approximately 250°F temperature. Table 3-1 lists all components and materials for both the Model S and Model E.

3.6 PERFORMANCE TRADEOFFS

The Maxometer force balance equation, Eq. (3.3), may be rearranged so that

$$F = qC_d A = \frac{1}{2}\rho V^2 C_d \cdot \frac{\pi D_d^2}{4} ,$$

and

$$V \cdot D_d = \sqrt{\frac{8F}{\pi C_d \rho}} \qquad (3.31)$$

or the product of the velocity times the disk diameter is a constant for a given air density (ρ), design spring force (F), and disk drag coefficient (C_d). The drag coefficient is a constant value when the Reynolds' number is well above 10^4 (Ref. 1). The product VD_d is also used in determining the Reynolds number (Re). Thus,

$$Re = \frac{V D_d}{\nu} \qquad (3.32)$$

Table 3-1

MAXOMETER COMPONENT MATERIALS

Item	Material		Remarks
	Model S	Model E	
Piston	Type 303 SS*	Type 303 SS*	
Spring Guide	Rulon J	Rulon J	low coefficient of friction
Piston Sleeve	Graphite	Graphite	low coefficient of friction
Orifice	17-4PH SS	17-4PIL SS	
Nose Cap	Silicon Glass	Aluminum	
Closure	Silicon Glass	Aluminum	
Closure Spring Guide	Rulon J	Rulon J	
Cylinder	Pyrex Glass No. 7740	Pyrex Glass	close tolerance bore
Rod	440C SS	440C SS	surface hardened
Disk	Silicon Glass SS	Silicon Glass Alum	withstand heat, lightweight
Compression Spring	Nickel Alloy Ni-Span-C	Ni-Span-C	constant expansion coefficient
Ball Cage	Rulon J	Rulon J	
Support Tube	Not Required	Aluminum	
Casing	Silicon Glass	Polycarbonate	
Bearing Shaft	Not Required	303 SS	
Cam	17-4PH SS	17-4PH SS	hard-high temperature
Cradle	316 SS	Not Required	
Stand	316 SS	Not Required	
Connector	303 SS	303 SS	
Spring Guide Tube	Rulon J	Rulon J	
Zero Adjust Rod	303 SS	Not Required	
Nut	303 SS	Not Required	
Spring Retainer	303 SS	Not Required	
Nut Bearing Lock	Not Required	Aluminum	
Upper Pipe Stand	Not Required	Aluminum	
Ball Return Spring	Be Cu	Be Cu	
Fin	Not Required	Aluminum	
Spacer	Not Required	Aluminum	
Ball	Ceramic	Ceramic	hard, high crush load
O-Ring	Silicon Compound	Silicon Compound	
Roll Pins	Stainless Steel	Stainless Steel	
Screws	Stainless Steel	Stainless Steel	
Knob	Stainless Steel	Not Required	

*Stainless Steel.

where

ν = air kinematic viscosity at $60^{\circ}F = 1.58 \times 10^{-4}$ ft^2/sec
= air kinematic viscosity at $1000^{\circ}F \simeq 7.8 \times 10^{-4}$ ft^2/sec

V = air velocity, m/sec

D_d = disk diameter, in.

Equating the above value to the minimum Re of 10^4, the VD_d product is 5.8 for air at $60^{\circ}F$ and 28.5 for air at $1000^{\circ}F$. This imposes a lower velocity limit for maintaining a constant C_d value as shown in Fig. 3-14. Measurements below this level may experience a velocity error as much as 30% due to drag coefficient variation. The drag coefficient may be as high as 2.0 at $Re \simeq 4 \times 10^2$ (from Ref. 1).

Other Maxometer instrument limits are determined by the lower friction threshold (force required to initiate piston motion) and the maximum spring force. Using design values, the VD_d product for these limits have been estimated at 8x4 or 32 for the friction threshold, and 135x4 or 540 for the maximum spring force (both evaluated at $60^{\circ}F$ ambient temperature). These limits are inversely proportional to the $\sqrt{\rho}$, or directly proportional to the square root of the ambient temperature ($^{\circ}R$). Thus, the limits shown in Fig. 3-14 may be modified for the particular temperature in question in this manner. The friction threshold is much higher than the Reynolds number threshold. Thus, the latter is not plotted in Fig. 3-14.

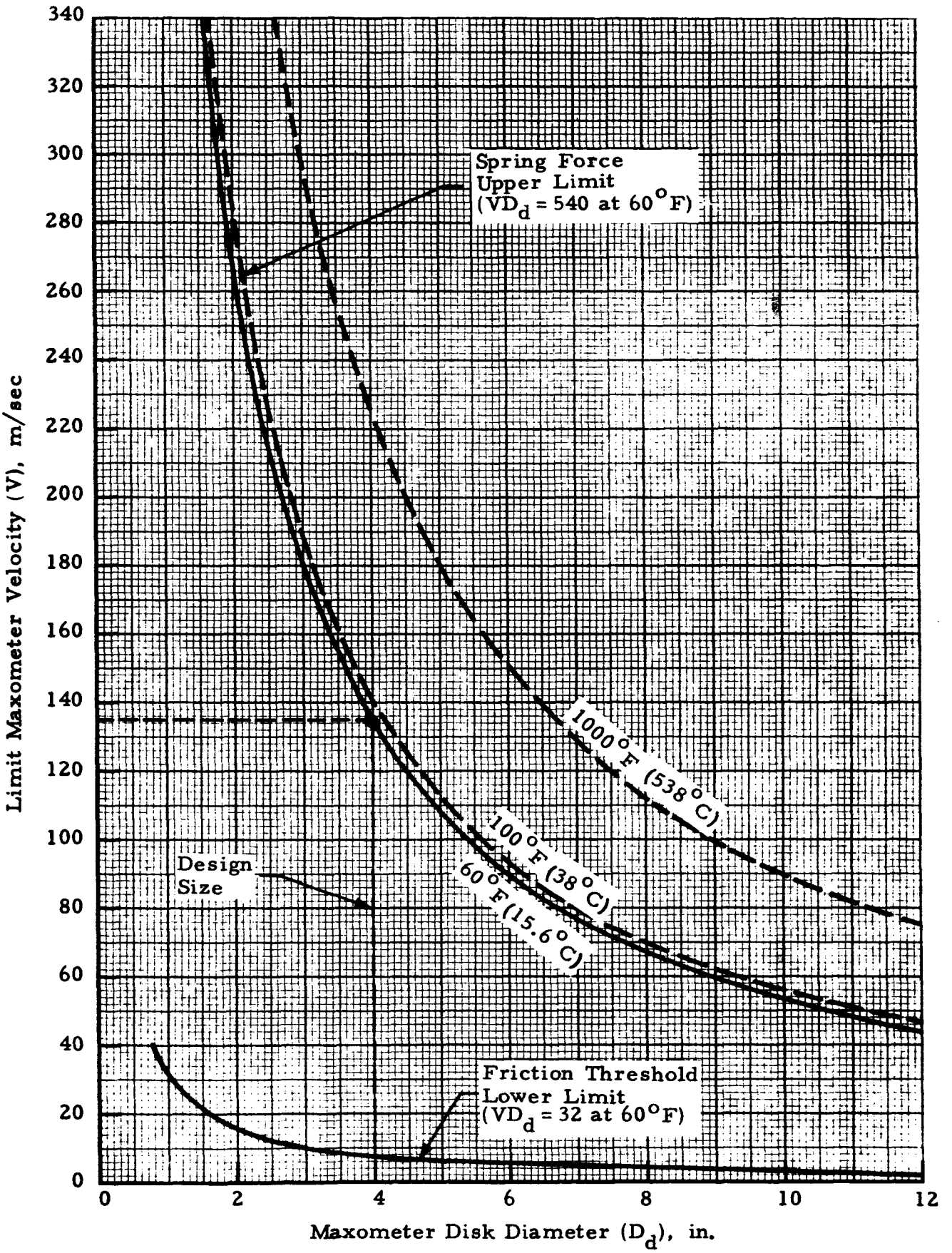

Fig. 3-14 - Maxometer Performance Limits for Various Disk Diameters

Section 4
MAXOMETER DEVELOPMENT

During the design, fabrication and calibration phases, a number of problems were encountered which were developed in nature and which required a number of minor design changes. None of the problems encountered affected the overall feasibility of the Maxometer concept. The major problem areas involved the springs, clutch mechanism, friction and the glass cylinder. Other more minor problems included difficulties in machining the silicon glass end pieces for the Model S configuration and pivot bearing looseness for the Model E configuration. These problem areas and resultant corrective action are discussed in the following sections.

4.1 SPRINGS

Initial studies indicated that a spring with nonlinear load-deflection characteristics was highly desirable in order to maintain the desired accuracy over the full range. Also, this would allow for a direct proportional relationship between velocity and displacement and hence facilitate readout. The use of nonlinear springs, however, was ruled out for three reasons:

- Cost – One precision spring would cost approximately $800, which defeats the concept of a low-cost expendable item.
- Accuracy – Repeatability from spring to spring would be approximately 4%; thus, to achieve ±5% accuracy reading would be highly improbable. Also, as indicated in Section 3.4.1, the resolution accuracy at high spring deflection is somewhat less than the linear spring.
- Size – According to Ref. 10, a spring that will produce accuracy readings of ±5% will require a free length of three times the stroke, making the overall length greater than is deemed feasible from an aerodynamic viewpoint of flow interference.

A Rolamite concept, an alternate means of obtaining nonlinear spring characteristics, was investigated from an analytical and small hardware model approach (Refs. 11 and 12). The analytical investigation showed that the concept could be used, but the model indicated that many development problems would have to be overcome. These problems range from thickness and tensioning of the band to sizing and guiding of the rollers. Thus, the nonlinear spring concept was discontinued in favor of a dual rate spring concept described in Section 3.

After assembly of the initial Maxometer configuration shown in Fig. 4-1, it was apparent that lateral deflection of the springs during engagement and compression was occurring and indicated a need for lateral support. This problem was solved by installing a sleeve in the piston assembly for guiding the low-rate spring, and by using a guide sleeve for the high-rate spring, as shown in Fig. 3-3. This change later resulted in minor friction problems as discussed in Section 4.3.

4.2 CLUTCH MECHANISM

The original ball clutch mechanism had the balls and ball return spring located in the piston. The clutching function was performed by the $2\frac{1}{2}$ deg slope in the piston, ball and cylinder wall (Fig. 4-1). Clutch release was performed by rotating one section of the piston relative to the other, thereby forcing the balls out of engagement due to the decreasing slot on the turning piston half. The two piston sections were spring loaded so that proper orientation was maintained when the rotated section was released. This device produced some sophisticated machine operations. However, this clutching mechanism imposed high localized loads on the Pyrex glass cylinder when deflecting the high-rate spring. The resultant radial loads fractured the glass (tension failure) and prompted the ball clutch analysis, described in Section 3.4.6.1. The Pyrex tubing was selected because it was readily available with a hard, smooth precision bore (1.0000 ± 0.0002 in.). New clutching concepts were investigated. Table 4-1 lists alternative schemes. The concept chosen was the disk-rod ball clutch, Fig. 3-3.

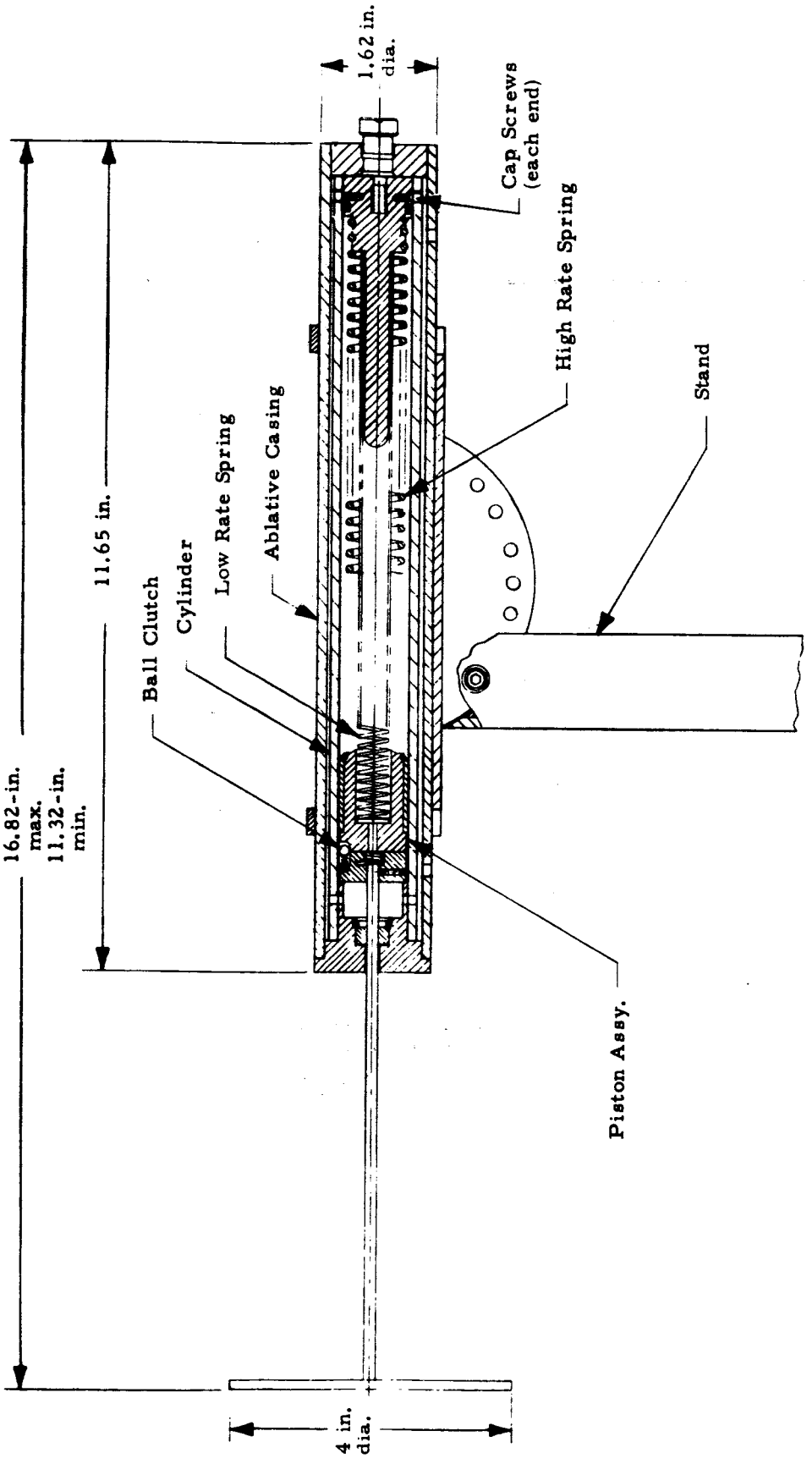

Fig. 4-1 - Initial Maxometer Configuration

Table 4-1

MAXOMETER CLUTCHING CONCEPTS

Concept	Description	Advantages	Disadvantages
High Strength-Hardened Tube	Replace pyrex glass tube with high-strength/tempered steel or Alumina tubing	Use existing clutching mechanism by replacing sapphire clutching balls with high-strength tool steel balls.	• Lack of transparent cylinder eliminates internal readout feature • Metal tube presents potential static electricity problems • Alumina and metal tubing are potentially expensive in order to meet precision i.d. requirements • Metal tube subject to brinelling from localised stresses
No-Clutch	Eliminate clutching and utilize other peak displacement measuring devices such as: 1. Friction or ball-clutching collar on disk rod 2. Wax coating on inside of piston cylinder with scribe marker on piston (Also felt tip ink marker)	Simpler mechanism Simple, reduced number of functioning parts	Subject to performance degradation from dust, and salt spray environment • Requires recoating or replacement of marked surface for each measurement • Wax coating increases piston friction or presents piston sealing problems
Disk-Rod Clutch	Eliminate piston clutching mechanism and replace with disk rod clutching mechanism	• May still utilize inexpensive, precision pyrex glass cylinder and internal readout • More compact • Easily accessible for resetting • Serves dual purpose as ball clutch and rod bushing	• Possible disk rod brinelling at high wind speeds, possibly requiring rod replacement

The advantages were numerous, and the primary disadvantage was not serious because replacement disk rods are not expensive and the high peak wind speeds are not expected at every reading. Also, the brinelling phenomenon (local dimpling from high localized stresses) may not interfere with subsequent peak wind speed measurements. This concept proved itself when the sapphire balls were replaced with ceramic balls. The sapphire balls fractured under the high point stress. Microscopic examination of the ceramic balls indicated no deformation or flattening after repeated usage. Also, the rod brinelling was detectable but did not compromise repeated usage.

4.3 FRICTION

Eccentric weight loading and slight deviations in alignment of the disk, rod and piston assembly caused excessive friction which compromised the low-speed characteristics of the initial Maxometer configuration (Fig. 4-1). This problem was solved by reducing the weight of the disk and piston assembly, by reducing the length of the piston carbon bushing, and by careful attention to alignment of the disk rod relative to the piston assembly. Additional relief from this problem was effected by the ball clutch redesign, in that any misalignment would be absorbed by the clutch mechanism.

After a series of Maxometer calibrations, it was determined that the ball clutch return spring breakaway force had a serious effect on the friction threshold for the disk-piston assembly. Early estimates for the required spring constant was 0.04 lb/in. Two of the Maxometers had a breakaway force of approximately 2 oz., while the other units were about 1 oz. All ball clutch springs were adjusted to maintain a 1/2 to 1 oz. range.

Incorporation of the spring guide design shown in Fig. 3-3 introduced an additional friction problem. For certain orientations, slight sagging of the high-rate spring caused increased friction when engaged by the low-rate spring guide. In most all cases, this was eliminated by rotating the assembly

about the longitudinal axis to minimize high-rate spring sag. Further work is recommended to eliminate this problem.

4.4 PYREX GLASS CYLINDER

Along with the glass cylinder breakage due to the original clutch mechanism, another problem became apparent — namely, how to effectively hold the glass ends. The original concept had four holes in each end of the glass, which aligned with four threaded holes in each end cap. Four socket head cap screws were used to attach each end cap to the glass cylinder. (See Fig. 4-1.) However, the tolerances maintainable on both the glass length, hole edge distance, and hole angularity pattern made it impossible to use more than two cap screws. Almost every mounting produced radial and point loadings which fractured the glass. The risk involved in using this arrangement was deemed impracticable, even though a unit was built and operated using only two screws in each end.

The next approach to this problem was to use heat shrinkable tubing between the glass and end cap. An aluminum ring bonded to the glass and a groove cut in the end cap provided additional surfaces for holding. The heat shrinkable tubing was applied and tested. The holding power proved to be sufficient, 1.4 times the anticipated maximum load, but was ruled out because long-term creep properties of the tubing was questionable and specific data were not available.

This problem was resolved by using tension rods between the two end caps as described in Section 3.4.6.3. By using this technique, the spring compressive loads are reacted by the tension rods. The glass cylinder is free of localized tensile stresses and will be required to take only the compressive loads from the rod pre-tension.

4.5 OTHER DEVELOPMENT EFFORTS

Certain items for improvement became apparent after fabrication had been started. One of these was that the stand provide pivoting capabilities so that three Model S units can be placed orthogonally from the same mounting reference plane. To do so requires a capability of compensating for the initial displacement of the disk-rod-piston assembly under its own weight. This was solved by coupling the low-rate spring directly to the piston while the opposite end is displaceable by a screw adjustment to put the spring in tension or compression for the proper compensation (depending upon instrument orientation with respect to vertical). See Fig. 3-3. In operation, the adjusting screw knob is turned while the instrument is in its operating position until a zero-scale reading is indicated. The clutch mechanism is disengaged during this adjustment. The Model E unit does not require the zero adjust mechanism, since it is used only in the horizontal plane.

The primary fabrication problem occurred with Model S unit components, primarily the two end caps (or closures). These were made from a silicon glass laminate to meet the high temperature requirements. This material was found to be difficult to machine, and, in several cases, the material parted parallel to the laminates. They were re-bonded with a high temperature adhesive. Further work is recommended to select a new material for these end caps. Several high temperature castable plastics should meet the requirements.

The pivot bearing for the Model E Maxometer (Fig. 3-2) was originally a single-row ball bearing configuration. Because of excessive looseness in the pivot, this was replaced by a double-row bearing configuration. During wind tunnel tests, the single-row configuration looseness apparently caused some minor flutter. The double-row configuration should solve this problem satisfactorily.

Section 5
MAXOMETER CALIBRATION TESTS

5.1 LABORATORY CALIBRATION

A laboratory force versus deflection calibration was required prior to the wind tunnel tests in order to properly evaluate the wind tunnel data. For the Maxometer these calibrations consisted of static force versus deflection measurements using precision dead weights and reading the Maxometer displacement directly. Figure 5-1 is a picture of the test apparatus. Initially the displacement was measured with a dial indicator. This was later replaced by a scale bonded to the glass cylinder in order to measure the piston displacement. Since the final reading is in the clutched position, the displacement was read after the weight was carefully removed. To further approximate actual environment, vibration was induced into the system by use of a saber saw mounted to the calibration table. The resultant calibrations for all units were very consistent. In Fig. 5-3, the linear characteristics are shown for the low and high ranges of all six units. The calibration data are presented in Table 5-1. The design characteristic, as may be computed from equations and data from Section 3.4.3, is between the mean value line and the minus 5% line shown in Fig. 5-3. Thus, excellent agreement was found between design and measured values.

Along with the vertical calibrations, a number of horizontal calibrations were conducted using a Hunter Spring Company Mechanical Force Gage, Model D-20-T. These data are the Model E data in Table 5-1 and are included in the plotted data in Fig. 5-3. The results of these data indicated very little difference between horizontal and vertical. Specifically, there was no detectable force difference at deflections above one inch and approached approximately 0.05 lb at zero deflection. This was attributed to eccentric friction loading of the disk-rod-piston assembly.

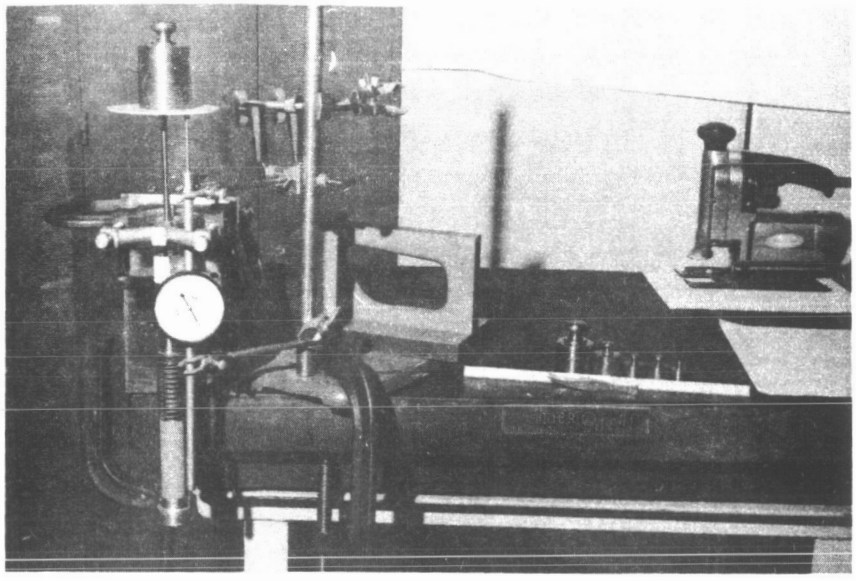

Fig. 5-1 - Laboratory Calibration Test Apparatus

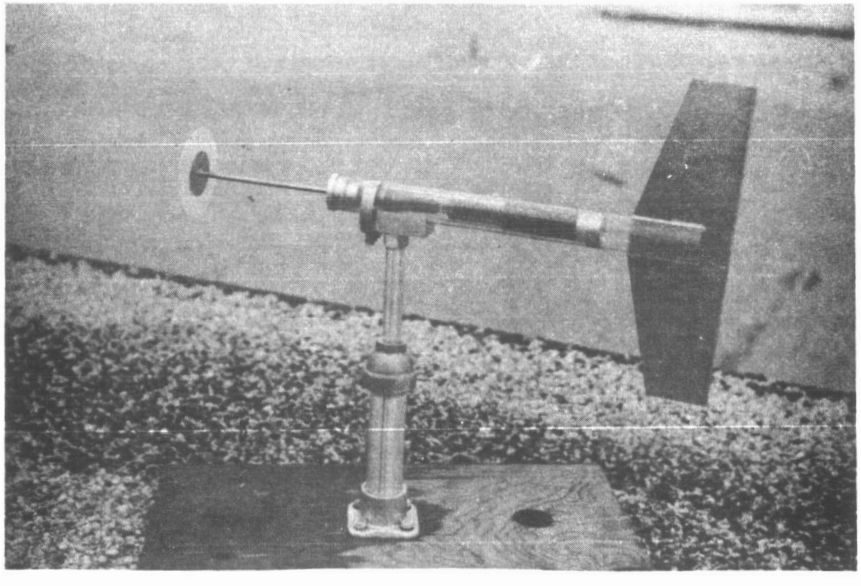

Fig. 5-2 - Model E Maxometer on Roof of Lockheed

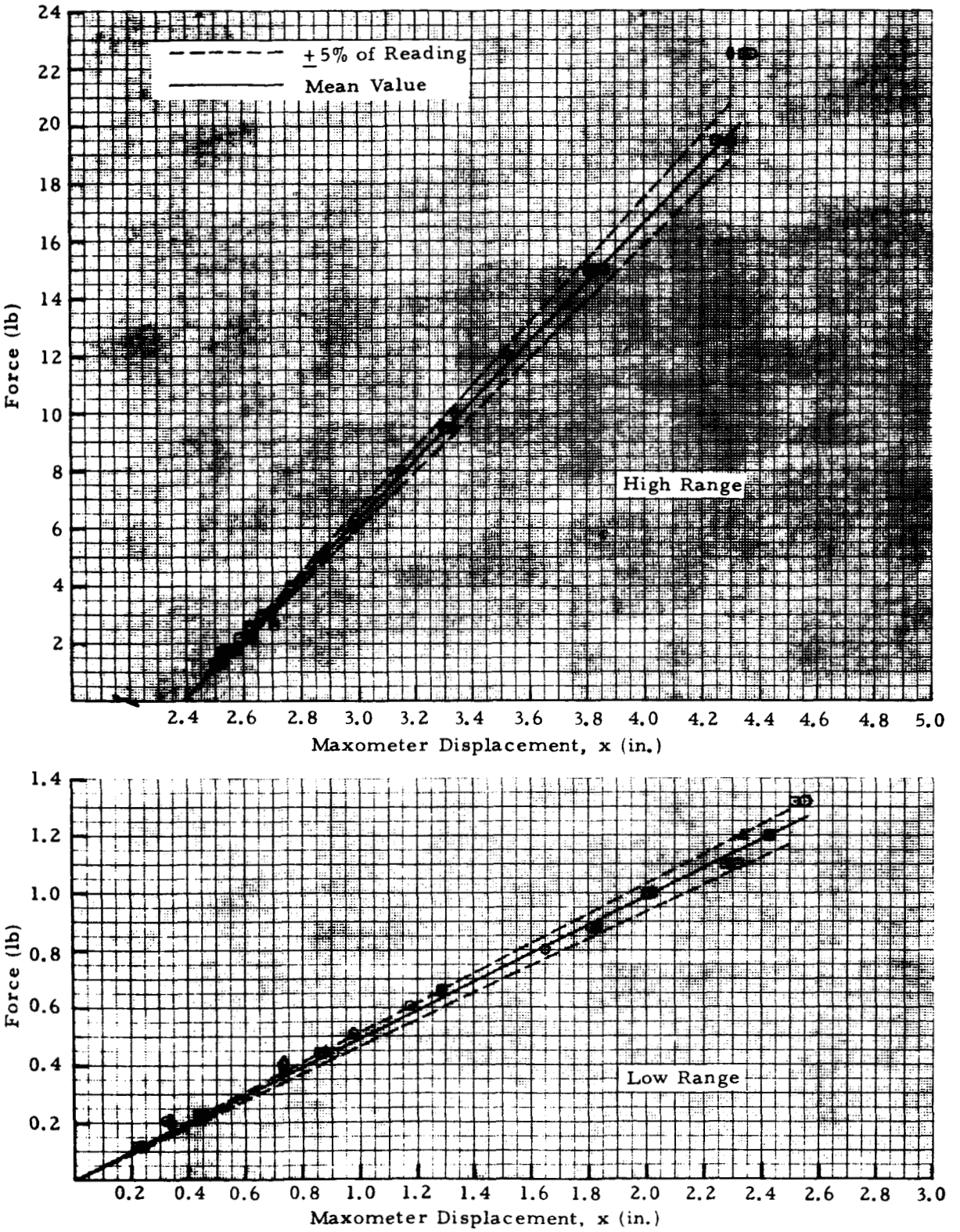

Fig. 5-3 - Maxometer Force versus Displacement Calibration

Table 5-1

CALIBRATION DATA (Static)

Unit → / Weight (lb) ↓	S1 Disp. (in.)	S2 Disp. (in.)	S3 Disp. (in.)
0.11	0.23	0.22	0.22
0.221	0.45	0.44	0.44
0.441	0.90	0.86	0.875
0.662	1.28	1.28	1.28
0.882	1.81	1.82	1.82
1.101	2.32	2.28	2.29
1.322	2.50	2.52	2.51
1.765	2.53	2.57	2.56
2.205	2.58	2.62	2.61
2.645	2.62	2.70	2.64
3.310	2.69	2.72	—
3.06	2.67	2.69	2.68
5.00	2.87	2.87	2.87
9.50	3.31	3.30	3.33
15.00	3.86	3.82	3.80
19.50	4.30	4.25	4.30
22.56	4.37	4.35	4.30

Unit → / Weight (lb) ↓	E1 Disp. (in.)	E2 Disp. (in.)	E3 Disp. (in.)
0.2	0.33	0.34	0.34
0.4	0.75	0.70	0.72
0.5	0.98	—	—
0.6	1.18	1.13	1.12
0.8	1.65	1.62	1.56
1.0	2.00	2.00	1.93
1.2	2.50	2.43	2.42

NOTE: Model S Calibration:
Vertical - No Reset - With Vibration

Model E Calibration:
Horizontal - With Force Gauge

The equations for the mean of the data shown in Fig. 5-3, based on the format of Eq. (3.18), are given below.

Low Range

$$q\,C_d\,A_d = 0.02 + 0.484x\,,\ \text{lb} \tag{5.1}$$

High Range

$$q\,C_d\,A_d = 10.28x - 24.45\,,\ \text{lb} \tag{5.2}$$

From these equations and Eq. (3.18), it was determined that the effective calibrated spring constants were $K_1 = 0.484$ lb/in. and $K_2 = 9.80$ lb/in. Also, it is noted that the low range has approximately a 0.02 lb friction threshold at zero displacement. Limitations of the calibration procedure did not permit a more accurate evaluation of the near zero values. A more accurate calibration technique is recommended. This would be especially useful in evaluating the friction differential between the horizontal and vertical positions.

Additional checks were made of the Maxometer to evaluate the threshold clutching force. To do this the Maxometer was rigidly held in a horizontal plane and the disk displaced by pushing on the disk center with a spring force gauge. Once a displacement had been reached, e.g., one pound, the force gauge was removed and the Maxometer clutch allowed to engage. Then, by pushing on the disk again, the piston was seen to move at or before the force gauge read the pre-set load, e.g., one pound. This procedure was performed with a Pelouze Mfg. Company Model 5T Tension Testing Scale, which has a five (5) pound full scale and one-ounce graduations. Using this technique, no detectable clutching threshold could be observed throughout the force range.

In addition to the laboratory tests, the first Model E Maxometer assembly was placed on the roof of Lockheed for a two-week period (Fig. 5-2). Daily observations of the piston displacement and weather conditions (rain, snow, temperature) were made and recorded. The primary conclusion drawn from these tests was that the Maxometer did function well under adverse conditions,

rain, snow and freezing temperatures. However, a protective covering over the ball-clutch area would be helpful in preventing the clutch from accumulating moisture and freezing. See comments in table below. Peak velocity values were computed from design and laboratory force calibration data. Comparison of the Maxometer data with data from the MSFC Meteorological Research Facility, six-miles distant, was favorable.

Period (1970)	Weather Cond.	Maxometer Reading (in.)	Temp. (^{o}F)	Peak Velocity (m/sec)	Remarks
1/23-1/26	Rain	0.53	40	15.2	
1/26-1/29 (0730)	—	0.47	~60	14.6	
1/29 (0730-0945)	Overcast	0.85	65	19.7	
1/29 (0945-1645)	Rain	0.60	40	16.2	
1/30 (0830	—	0.45	29	13.9	
1/30-2/2 (1100)	Rain	1.06	~60	22.0	
2/2-2/3 (1130)	Freezing Rain/Snow	0.50	16	14.3	Clutch frozen to prevent reset but still had positive clutching action
2/3-2/4 (1530)	Cold	0.38	7 to 20	12.5	

5.2 WIND TUNNEL TESTS

5.2.1 Test Description and Results

Wind tunnel tests of four Maxometers (three Model S and one Model E) were conducted in the High-Speed 7 by 10 foot Wind Tunnel located at NASA-Langley, Virginia, 23-28 March 1970. These tests were for static and dynamic calibration of the Maxometers under wind load conditions.

The 7 x 10-foot wind tunnel has a test section adequate in size to mount all four sensors tested simultaneously. To reduce the wall boundary layer effects and obtain a more accurate dynamic pressure, three units were mounted on 14-in. stands so that they were nearly on tunnel centerline. The fourth unit was mounted to the wall with no standoff; see Fig. 5-4 and 5-5.

A finalized run schedule includes a total of 44 runs, and four of these were repeatability runs. See Table 5-2. The two parameters varied were velocity and angle of attack (or weathervane angle). Tests of 15 different velocities were conducted. A full coverage of the Maxometer velocity range was attempted. However, the lower velocities (8-20 m/sec) were unobtainable because of the wind tunnel limitations. A number of velocities were only one meter per second apart to check the sensitivity or clutching threshold at various velocity levels. For the Model S, six angles of attack were tested at two velocities. The Model E had five weathervane angles. A special case where the Maxometer is pre-set to a velocity and then a higher velocity is applied was run for four cases.

Simulated step function wind speeds were applied to the Maxometers by using a retention and instantaneous release scheme for both the disk and Model E pivot as shown in Figs. 5-6 and 5-7. An electrical exploding wire provides instantaneous release for the balsa wood rod holding the disk (Fig. 5-6) and the lanyard for the pre-set weathervane angles (Fig. 5-7).

The wind tunnel test results are given in Table 5-3. Maxometer displacements were obtained from visual inspection of each instrument after each test run. Corresponding wind tunnel data – velocity, temperature, density and dynamic pressure – were obtained from instrumentation provided by NASA-Langley Research Center. Besides the data in Table 5-3, high-speed motion picture film was used to record the weathervaning response of the Model E instrument. These data are presented in graphical form in Section 5.2.4.

Table 5-2

MAXOMETER RUN SCHEDULE

Run Number	Model Series**	Preload Velocity (m/sec)	Final Velocity (m/sec)	Angle of Attack (deg) Model S	Weathervane Angle (deg) Model E
4	S1, S2, S3, E1	0	20	0	0
5	↓	↓	25	↓	↓
6			30		
7		30	31		
8		31	32		
9		32	33		
10		0	40		
11		40	42		
12		0	60		
13		↓	80		
14			100		
15		100	103		
16		0	120		
17		120	124		
18		0	140		
19		0*	30		
20	↓	0*	80		
21		0*	100		
22	S1, S2, S3	0*	120		
23	S1, S2, S3, E1	10*	30		
24	↓	40*	80		
25		60*	100		
26		60*	120		
27		0	40		
28		↓	60		
29			80		
30			120	↓	↓
31			100	30	10*
32			40	30	10*
33			100	60	20*
34			40	60	20*
35			100	15	30*
36			40	15	30*
37			100	90	60*
38			40	90	60*
39			40	75	90*
40	↓	↓	100	75	90*
41			100	45	135*
42	S1, S2, S3		40	45	—
43	↓	↓	20	0	—
44			25	0	—

*Unit preset and instantaneously released when final velocity has been reached.

**The letter designates type model and the number designates unit series.

Table 5-3

WIND TUNNEL DATA SHEET

Run No.	Date and Time	Maxometer Displacement (in.) ⊙ Model E1	△ Model S1	⊙ Model S2	⊡ Model S3	Wind Tunnel Data (Note 1) Velocity m/sec	Temp. ^{o}F	Density $\frac{lb\text{-}sec^2}{ft^4}$	Dynamic Pres. $\frac{lb}{ft^2}$	Remarks
4	3/25/70 PM	1.28	1.01	0.96	0.95					Note 2
5	Wednesday	2.08	1.89	1.73	1.76	26.966	63.406	0.00235	9.196	p. 5-10
6		2.52	2.49	2.53	2.54	32.988	65.474	0.00234	13.688	
6/1		2.52	2.49	2.52	2.53	32.886	65.781	0.00233	13.589	
6/2		2.52	—	2.51	2.51	32.752	65.386	0.00234	13.489	
7		2.54	2.495	2.54	2.54	34.322	62.614	0.00235	14.885	
8		2.55	2.52	2.55	2.56	34.927	63.362	0.00234	15.385	
9		2.555	2.52	2.56	2.56	35.925	64.418	0.00234	16.233	
10		2.65	2.61	2.65	2.65	43.868	65.386	0.00233	24.095	Note 3
11	3/26/70 AM	2.68	2.65	2.68	2.68	45.129	61.075	0.00233	25.567	
12	Thursday	2.995	2.94	2.95	2.97	64.936	62.878	0.00230	52.261	
13		3.45	3.36	3.40	3.40	85.989	68.421	0.00225	89.419	
14		4.06	3.96	4.00	4.00	109.008	70.708	0.00219	139.997	
15		4.20	4.10	4.14	4.10	112.545	76.118	0.00216	147.404	
16		4.67	4.63	4.67	4.66	138.277	79.725	0.00211	199.989	Note 4
17		4.67	4.63	4.67	4.67	137.796	83.904	0.00208	212.514	
18		4.69	4.65	4.70	4.70	157.098	87.511	0.00202	268.188	Note 5
19	PM	2.52	2.50	2.54	2.54	33.512	71.940	0.00228	13.811	
20		3.46	3.36	3.40	3.40	87.389	76.030	0.00220	90.431	
21		4.03	4.00	3.96	3.90	109.911	79.901	0.00214	139.469	
22		—	4.49	4.56	4.56	132.934	84.871	0.00207	196.511	Note 6
23		2.52	2.49	2.53	2.54	33.368	77.218	0.00225	13.451	
24		3.46	3.35	3.42	3.45	88.429	82.980	0.00216	90.823	
25	3/27/70 AM	4.05	3.92	3.995	4.02	107.329	60.778	0.00226	139.976	
26	Friday	4.67	4.59	4.67	4.67	129.868	64.958	0.00219	199.205	
27		2.66	2.61	2.67	2.67	42.746	57.786	0.00238	23.381	
28		2.99	2.91	2.98	3.00	64.814	60.030	0.00234	52.818	
29		3.50	3.37	3.43	3.45	85.728	60.822	0.00231	91.255	
30		4.67	4.62	4.67	4.67	130.263	68.346	0.00219	199.585	
31		4.08	3.97	4.04	4.08	108.073	67.334	0.00223	140.428	
32		2.65	2.63	2.66	2.60	43.031	62.846	0.00235	23.443	
33	PM	4.07	4.13	4.06	4.14	108.098	67.862	0.00223	140.377	Note 6
34		2.67	2.65	2.67	2.70	43.618	66.058	0.00234	23.932	Note 4
35		4.07	3.97	4.00	4.05	108.169	71.954	0.00221	139.367	Note 7
36		2.67	2.63	2.65	2.69	43.164	69.094	0.00232	23.276	
37		4.24	0.18	0.01	0.00	108.247	70.238	0.00223	140.362	
38		2.75	0.01	0.01	0.00	43.499	68.346	0.00233	23.679	
39		2.74	2.50	2.50	2.56	44.191	67.510	0.00233	24.474	
40		4.37	3.25	3.23	3.23	107.808	71.866	0.00221	138.511	Note 8
41	3/28/70 AM	—	4.05	4.20	4.25	106.461	59.491	0.00228	139.086	Note 9
42	Saturday	—	2.72	2.76	2.80	48.500	57.028	0.00238	30.178	
43		—	0.98	0.79	0.80	21.719	59.931	0.00239	6.075	Note 10
44		—	0.46	0.25	0.25	18.646	59.271	0.00239	4.475	Note 10

NOTES TO TABLE 5-3

Note 1. Tunnel data are as received from NASA-Langley's Data Reduction program.

Note 2. No wind tunnel data were received from NASA-Langley.

Note 3. The Maxometer readings after Run 10 were recorded at the end of the working day. The next morning (approximately 16 hours later) the readings were noted and found to be the same.

Note 4. After Run 15, it was noted that the S1 model had an excessive amount of disk-rod wobble. After Run 16, Model S1 was read and then disassembled. The problem was located and fixed — the orifice to connector thread had been unscrewed. Model S2 had similar problem after Run 34.

Note 5. During Run 18, the fin on Model E1 came loose and separated from the model. A new fin was made by NASA-Langley along with a fix — balsa wood plug and screws to hold fin and plug in casing.

Note 6. First attempt on each of these runs was aborted due to Model E1 being released prematurely. This was caused by failure of the bond between the electrical terminal block and fixture. For Run 22 Model E1 was removed, since S1, S2 and S3 would record identical data as E1.

Note 7. First attempt at running had to be aborted since electrical wire holding E1 model weathervane lanyard pulled loose.

Note 8. The lanyard holding E1 model weathervaned broke, aborting first run. The lanyard was replaced with a higher breaking strength cord (250 lb).

Note 9. Original Run 41 called for Model E1 to be weathervaned to 135 deg and a velocity of 100 m/sec. This run was aborted because of the high loading on the bearing shaft of the weathervane mechanism with subsequent bending. Run 41 was changed as per run schedule, negating any further testing of Model E1.

Note 10. Runs 43 and 44 data apparently were reversed during the data reduction. The data as recorded in Table 5-3 are reversed from the order per NASA-Langley data reduction printout.

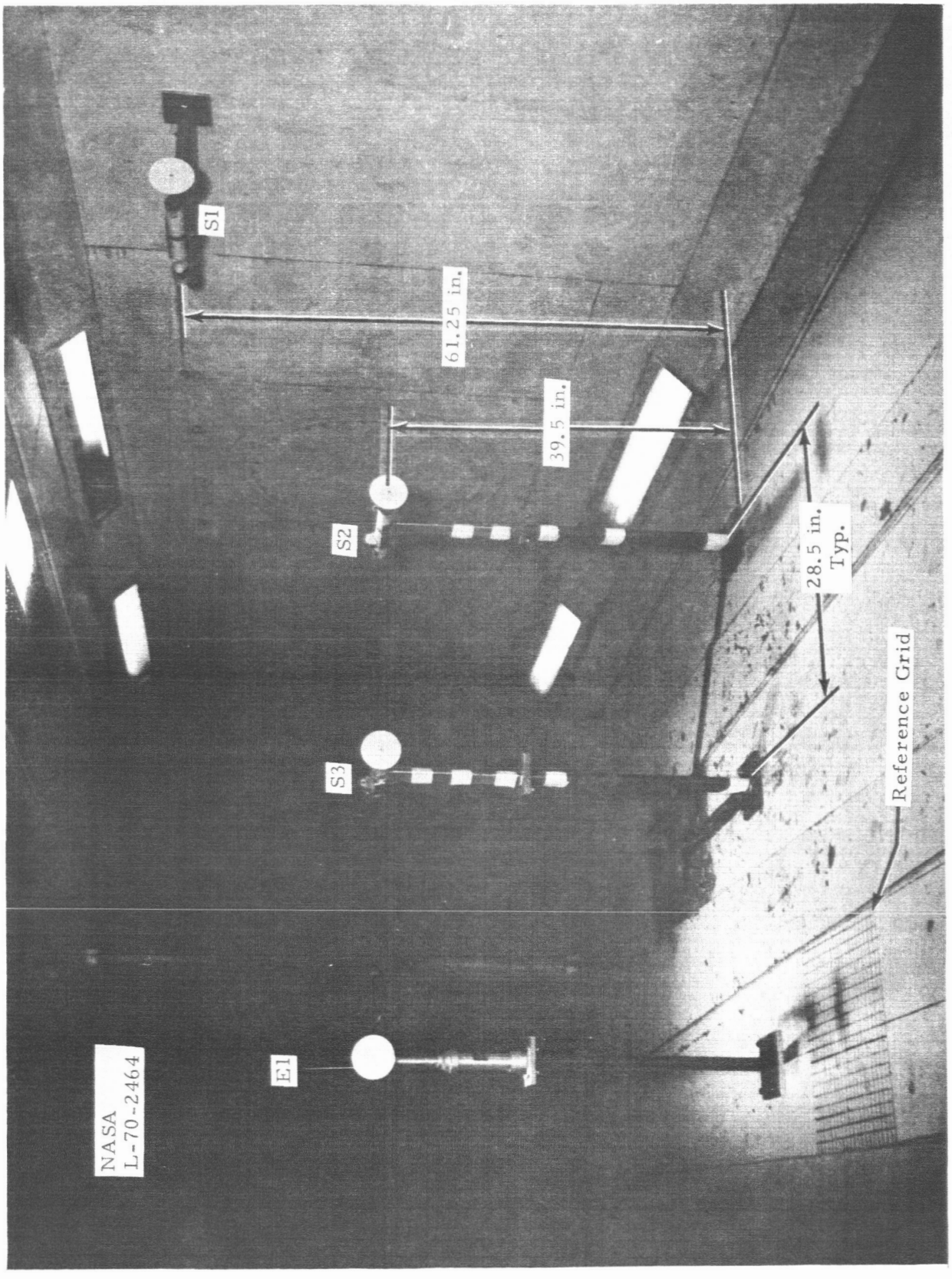

Fig. 5-4 - Maxometer Installation in NASA-Langley 7 by 10-Foot High Speed Wind Tunnel (Front View)

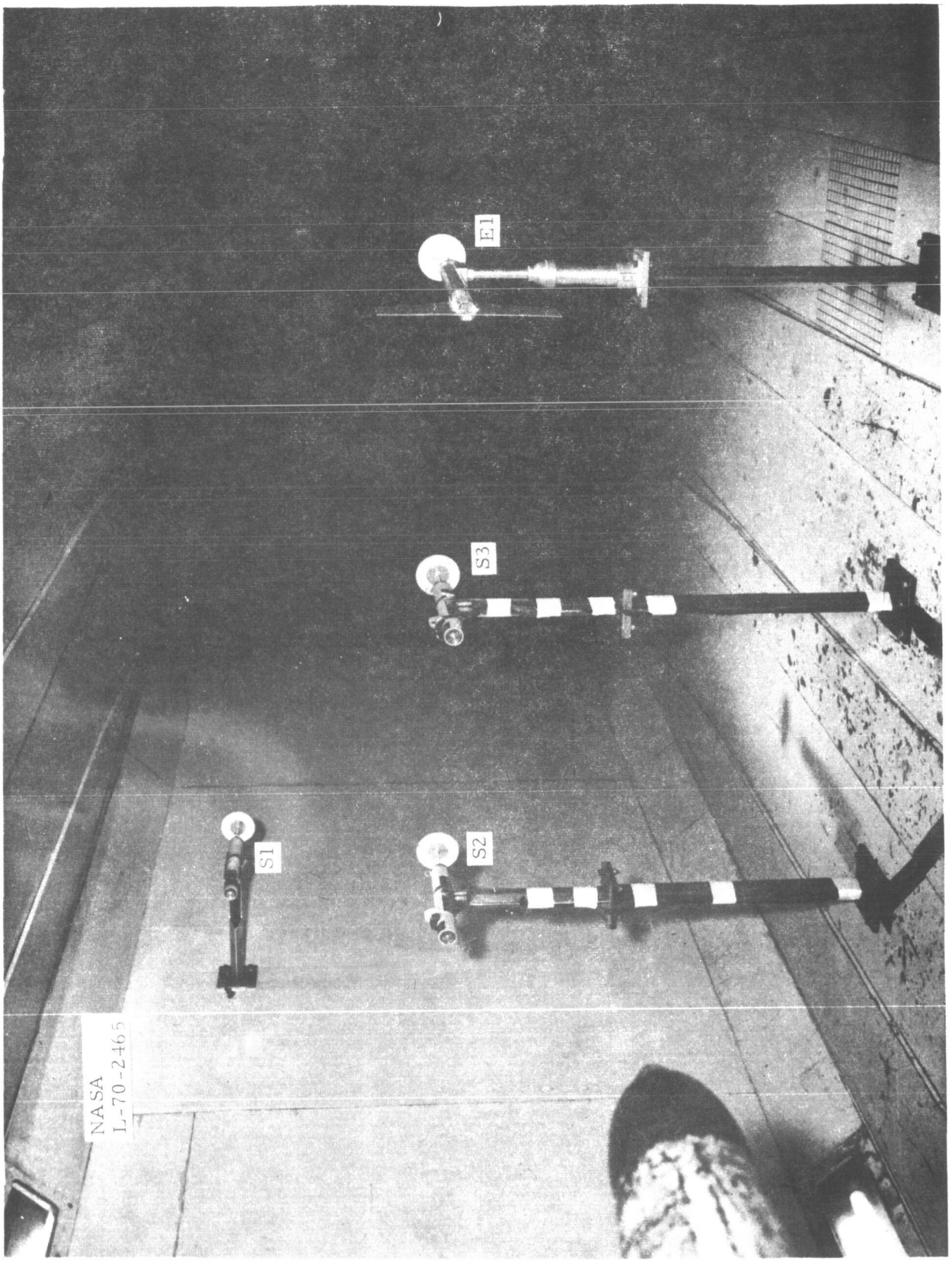

Fig. 5-5 - Maxometer Installation in NASA-Langley 7 by 10-Foot High Speed Wind Tunnel (Aft View)

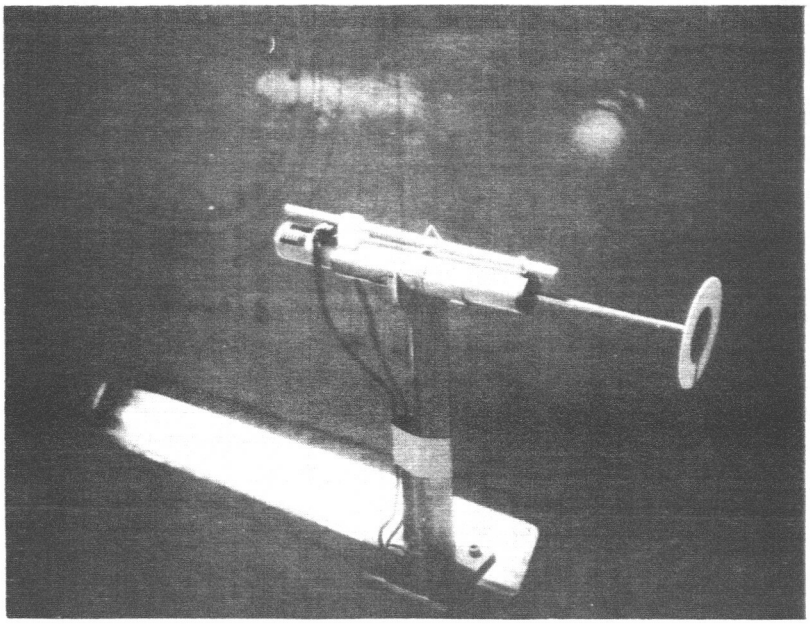

Fig. 5-6 - Model S Maxometer with Disk Retention Release Mechanism

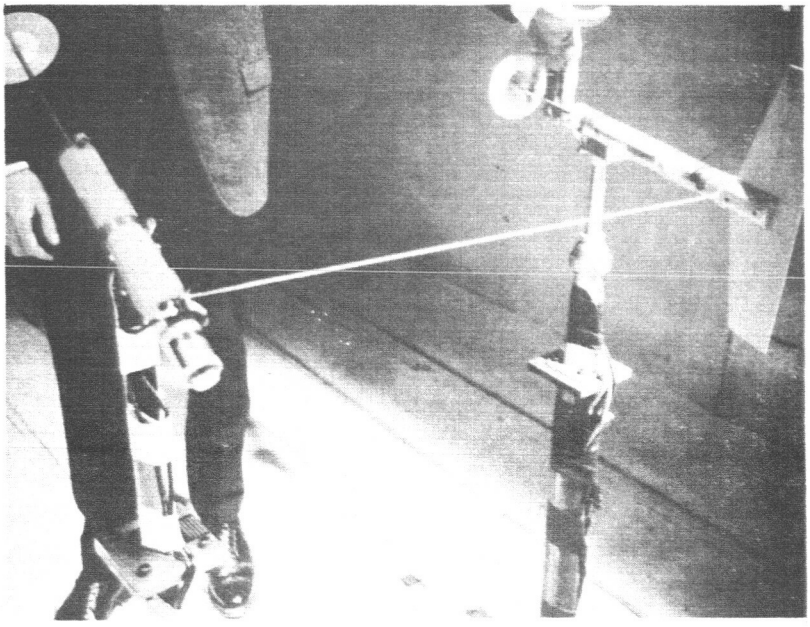

Fig. 5-7 - Model E Maxometer with Lanyard Weathervaning Retention Release Mechanism

5.2.2 Analysis of Dynamic Pressure Data

The Maxometer is basically a dynamic pressure measuring instrument. Therefore, the dynamic pressure data in Table 5-3 were the primary data for analysis. Of specific interest was the dynamic pressure versus Maxometer displacement relationship for each instrument as plotted collectively in Fig. 5-8. Some pertinent observations of these data are:

- As expected from the design data (Fig. 3-12), the test data shows a truly linear q versus x relationship, and the maximum test data scatter appears to be $\pm 5\%$ of mean reading. Thus, the velocity accuracy may be on the order of ± 2 - 3% of reading. (See Section 3.4.1.)

- The unit-to-unit variation for a given test appears to be very small – approximately $\pm 3.5\%$ of reading maximum. Models S2 and S3, mounted in close proximity, had a maximum variation of $\pm 1\%$ of reading for a given test.

- There was no perceptible variation from the dynamic (step function) tests and the steady-state tests. Thus, the dynamic response appears to be very good. (See Section 5.2.5.)

- Weathervaning apparently had no perceptible affect on the measurement of dynamic pressure.

- A dynamic pressure threshold at zero Maxometer displacement is approximately 3.3 lb/ft^2. This appears unusually high. However, no test data in the lower dynamic pressure values were available to verify this. More tests should be conducted in the 0 to 10 lb/ft^2 dynamic pressure range to more precisely determine this threshold and the low range calibration.

- The instrument drag coefficient appears to be somewhat higher than the design value, since the displacements for given dynamic pressure values were consistently higher than the design values.

Data plotted in Fig. 5-8 do not include those for angles of attack higher than 20 deg. Angle-of-attack effects are discussed separately in Section 5.2.3.

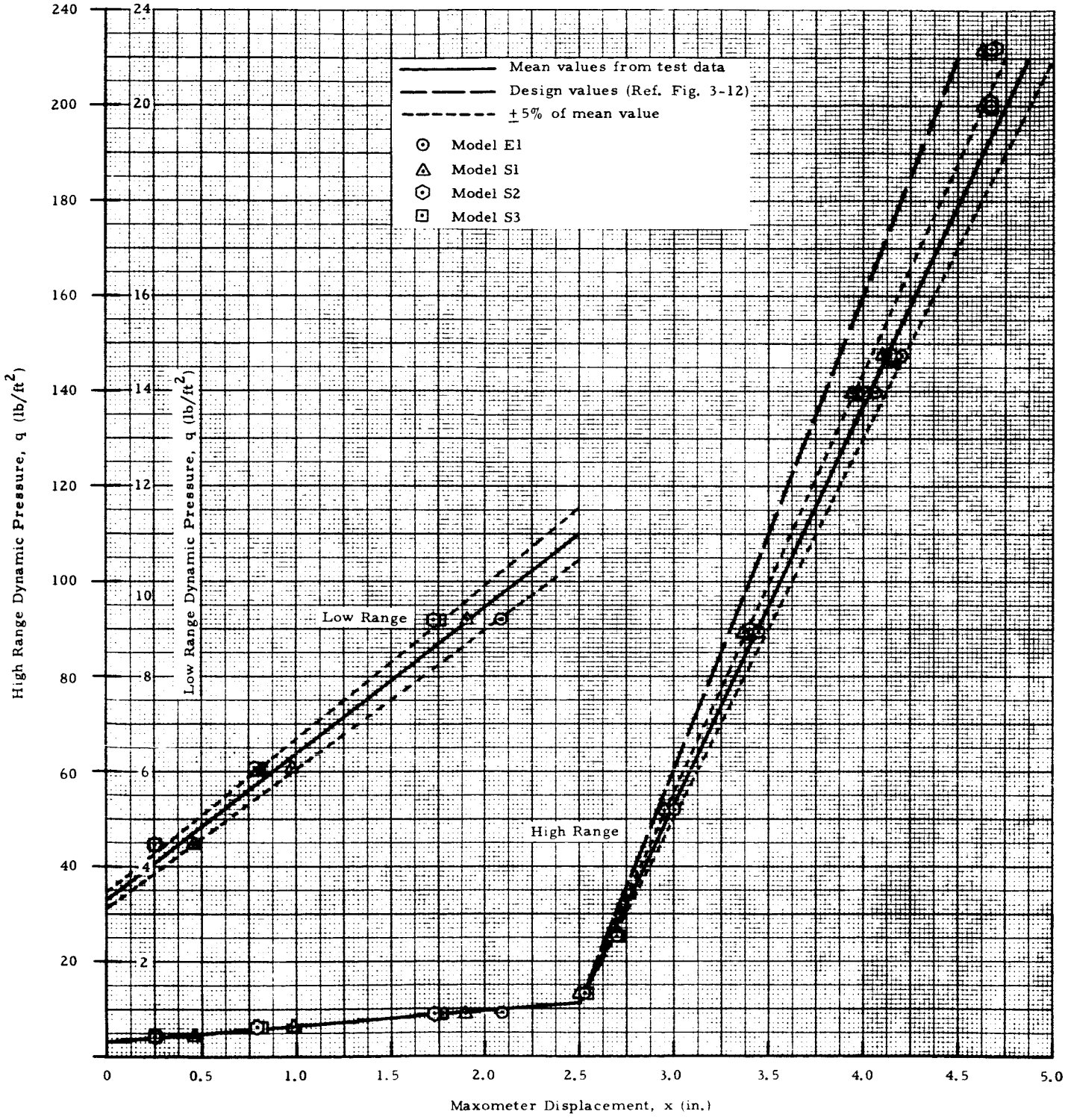

Fig. 5-8 - Maxometer Dynamic Pressure versus Displacement Test Results

The equations for the mean dynamic pressure characteristics shown in Fig. 5-8 are:

Low Range

$$q = 3.3 + 3.08x, \quad lb/ft^2 \tag{5.3}$$

High Range

$$q = 84x - 199, \quad lb/ft^2 \tag{5.4}$$

Comparing the constants in these equations with those in Eqs. (5.1) and (5.2), the effective drag coefficient (C_d) is 1.79 for the low range and 1.40 for the high range. This effective coefficient undoubtedly compensates for varying amounts of friction and reflects a discrepancy in the low range. Using these constants and the constants developed in Section 5.1, the following constants are summarized for use in the Maxometer performance equations, Eqs. (3.18) through (3.21):

K_1 = low range spring constant
= 0.484 lb/in.

K_2 = high range spring constant
= 9.80 lb/in. for $x_1 > 2.50$
= 0 for $x_1 < 2.500$

x_1 = low range displacement to high range spring contact
= 2.500 in. (63.5 mm)

C_d = effective disk drag coefficient
= 1.79 (low range)
= 1.40 (high range)

A_d = disk frontal area
= 0.0872 ft^2

q_o = additional dynamic pressure threshold for low range only
= 3.3 lb/ft^2

R = air gas constant
= 1716 $ft^2/sec^2-{}^oR$

Combining Eqs. (3.2), (5.3) and (5.4), the equations for Maxometer velocity versus displacement are:

Low Range

$$V = \sqrt{\frac{2RT}{144P}(3.3 + 3.08x)},$$

$$V = 8.87\sqrt{\frac{T}{P}(1 + 0.934x)}, \quad \text{ft/sec} \tag{5.5}$$

where $x \leqq 2.50$ in. displacement. Also,

$$V = 2.7\sqrt{\frac{T}{P}(1 + 0.0368x)}, \quad \text{m/sec} \tag{5.6}$$

where $x \geqq 63.5$ mm displacement.

High Range

$$V = \sqrt{\frac{2RT}{144P}(84x - 199)},$$

$$V = 44.5\sqrt{\frac{T}{P}(x - 2.37)}, \quad \text{ft/sec} \tag{5.7}$$

where $x \leqq 2.50$ in. displacement. Also,

$$V = 2.7\sqrt{\frac{T}{P}(x - 60.2)}, \quad \text{m/sec} \tag{5.8}$$

where $x \geqq 63.5$ mm displacement.

Units for temperature, T, and atmospheric pressure, P, are ^{o}R and lb/in^2, respectively. A standard day temperature and pressure of $520^{o}R$ and 14.7 psia, respectively, are assumed. The Maxometer velocity versus displacement relationships for these conditions are illustrated in Fig. 5-9. Also, the extreme temperature condition of $1000^{o}F$ is shown. As the graph indicates, the minimum velocity is approximately 16.5 m/sec at $60^{o}F$, and the maximum velocity exceeds 200 m/sec at $1000^{o}F$.

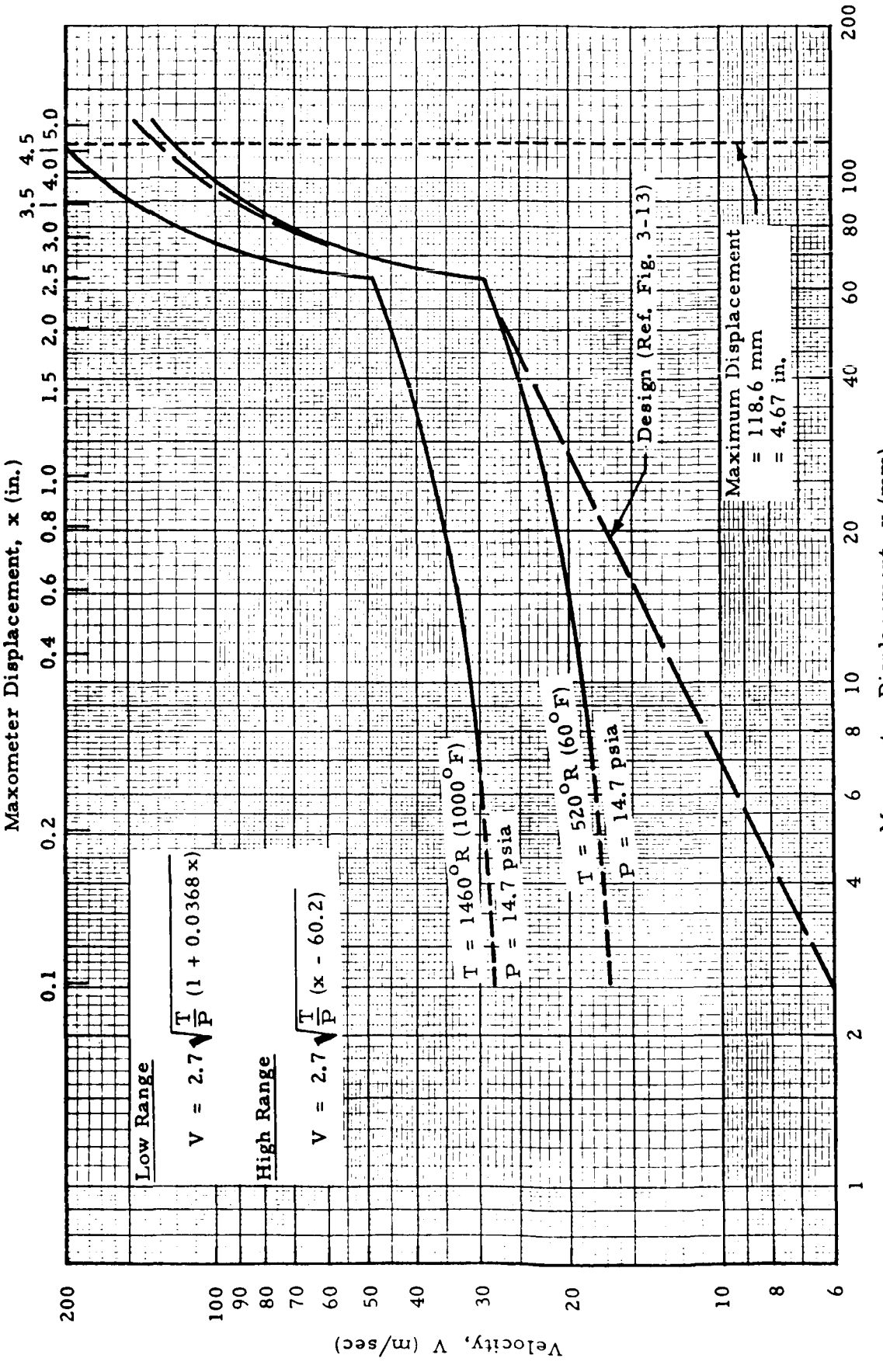

Fig. 5-9 - Maxometer Velocity vs Displacement

It is noted that the performance characteristics do not meet the 8 m/sec at 60°F minimum velocity threshold specified in Section 2. The discrepancy is also seen by comparison with the design curve in Fig. 5-9. NASA-Langley wind tunnel personnel cautioned that the data at 20 m/sec or below have questionable accuracy. This may be the primary reason for the discrepancy. More wind tunnel tests in the low q range (0 - 10 lb/ft^2) are required to verify this. It is noted that the laboratory force versus deflection calibration did not indicate serious friction problems in the low range. As an example, using the low range calibration, Eq. (5.1), a $q_o = 3.3$ and a $C_d = 1.79$, the equivalent Maxometer displacement is over one inch.

5.2.3 Angle of Attack (Model S)

The effects of angle of attack are best expressed graphically as shown in Fig. 5-10. With the two test velocities (dynamic pressure) held constant, the effect of angle of attack is shown by change of piston displacement. There is little effect due to change of angle up to 30 deg. Between 30 deg to 60 deg, greater piston displacement represents an increased negative coefficient of lift for the disc. The increase in lift is greater than the decrease in drag. Maximum displacement occurs at approximately 45 deg, which at the higher dynamic pressure represents an increased displacement of 4.5%.

The effects at the lower dynamic pressure are less pronounced with a maximum displacement error of 3.0% at approximately 45 deg. At angles greater than 60 deg, the lift and drag decrease rapidly for both dynamic pressures.

5.2.4 Weathervane Response (Model E)

The response of the Model E Maxometer was analyzed by reducing the film from the tunnel overhead and side camera. The overhead camera was mounted behind and slightly to one side of centerlines through the model pivot point. A grid placed on the tunnel floor ahead of the Model E unit served as a reference for the overhead camera. (See Fig. 5-4.) With the location of

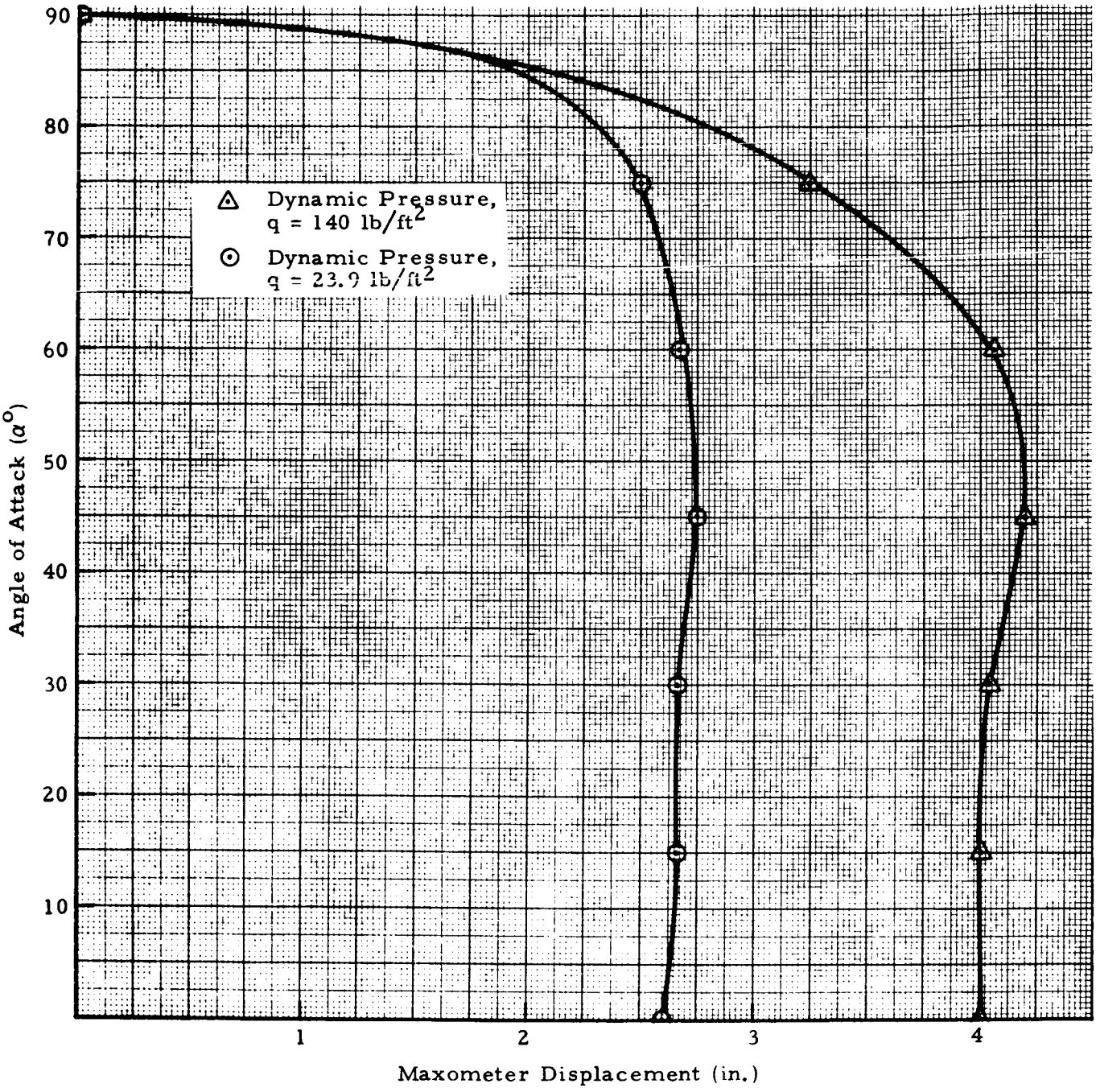

Fig. 5-10 - Effect of Angle of Attack on Maxometer Displacement at Constant Dynamic Pressure

the camera known with respect to the model, the elliptical pattern of a fixed point across the grid is reduced to angle of attack relative to the free stream.

In reviewing the data, two anomalies were uncovered as outlined below:

- The actual angle of attack at release was less than preset angle. This difference was caused by flexibility or stretch in the restraining lanyard and the location of the tiedown points (i.e., for 90 deg preset actual release angle approximately 70 deg).
- The second major anomaly was an apparent damping ratio of approximately 0.2 instead of the theoretical value of approximately 0.60.

The second major anomaly prompted a review of the initial theoretical data, and this revealed errors in basic equations as discussed in Section 3.4.7. In addition, during the tunnel test, the fin was lost and had to be replaced. When the repair was accomplished, an additional mounting block was added, which increased the inertia of the system from 0.0146 to 0.0179 slug-ft^2. Therefore, correcting for the errors in Ref. 8 and the change in inertia,

$$\lambda_N = 27.5 \text{ ft/cycle}$$

$$\delta_r = 0.228$$

$$f = 16.5 \text{ cycles/sec}$$

The actual damping ratio of the system is found by determining the rate of decay of oscillation. The rate of decay is best expressed by the logarithmic decrement (σ) or the logarithm of the ratio of any two successive amplitudes.

Expressed mathematically, the log decrement is:

$$\sigma = \ln \frac{\theta_1}{\theta_2} = \delta \, \omega_N \, \tau \qquad (5.9)$$

since $\tau = 2\pi/\omega_N\sqrt{1 - \delta_r^2}$ then:

$$\sigma = \frac{2\pi\delta_r}{\sqrt{1 - \delta_r^2}} \tag{5.10}$$

where

σ = log decrement

δ_r = damping ratio

τ = period

ω_N = natural frequency

The amplitude ratio is

$$e^{\sigma} = \frac{\theta_0}{\theta_1} = \frac{\theta_1}{\theta_2} = \ldots = \frac{\theta_{N-1}}{\theta_N}$$

or

$$\sigma = \ell n \frac{\theta_1}{\theta_2} + \ell n \frac{\theta_2}{\theta_3} + \ldots + \ell n \frac{\theta_N}{\theta_{N+1}}$$

For N cycles

$$\sigma = \frac{1}{N} \ell n \frac{\theta_1}{\theta_{N+1}} \tag{5.11}$$

From Eq. (5.10) it may be seen that

$$\delta_r^2 \left[\left(\frac{2\pi}{\sigma}\right)^2 + 1 - \frac{1}{\delta_r^2}\right] = 0$$

and for the nontrivial case, then

$$\delta_r^2 = \frac{1}{\left(\frac{2\pi}{\sigma}\right)^2 + 1}$$

$$\delta_r \cong \frac{\sigma}{2\pi} \qquad (5.12)$$

Two runs were chosen as typical in determining the actual damping ratio. The two runs, No. 37 and No. 39, represent the velocity extremes and different angles of attack at release. A graphical representation of the two runs is shown in Fig. 5-11. Analysis of these runs reveals the following data.

Parameter	Run No. 37	Run No. 39
Preset Angle, θ_i	60 deg	90 deg
Release Angle, θ_R	29.2 deg	68.6 deg
Test Velocity, V	108.2 m/sec	44.2 m/sec
Log Decrement, σ	1.45	1.28
Damping Ratio, δ	0.231	0.204

The test data then approximates the corrected theoretical value of $\delta = 0.228$.

The initially desired damping ratio of 0.6 can be obtained by increasing the fin area to 1.36 ft^2. Maintaining an aspect ratio of four, the span would be 2.33 ft.

The present fin configuration is sufficient to correct for a 90-deg wind direction change (i.e., reach an attitude parallel to gust) in less than 0.125 sec. The maximum overshoot angle is approximately 30 deg in the worst case, and therefore angle-of-attack error can be assumed to be negligible. (See Section 5.2.3.)

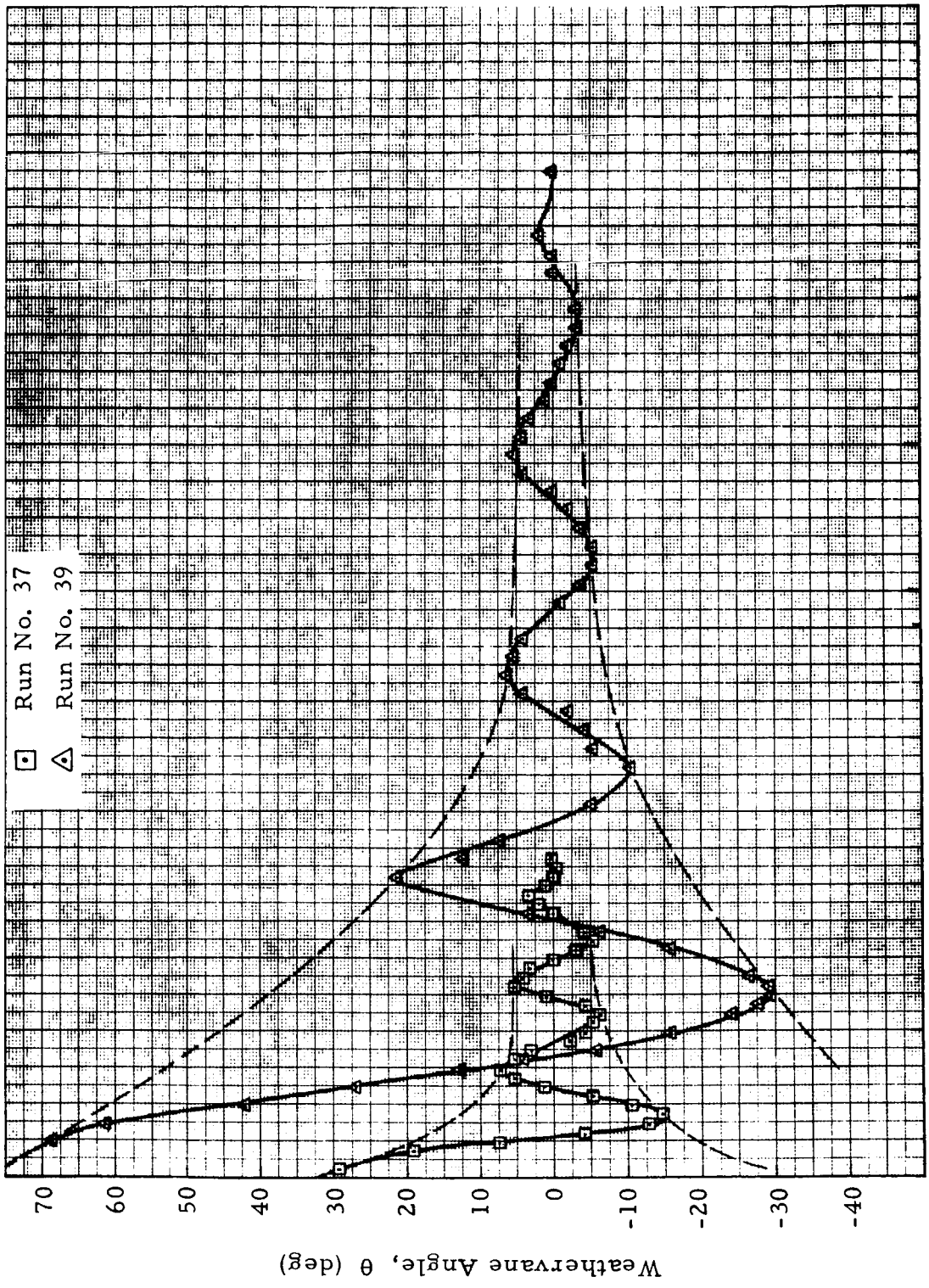

Fig. 5-11 - Model E Maxometer Weathervane Response

Since the maximum gust rise time expected is 0.250 sec, the present weathervane response is quite sufficient for accurate peak wind readings. The greatest Δt recorded for the Model E to stabilize (90 deg, 40 m/sec run) was 0.856 sec.

5.2.5 Maxometer Response

The Maxometer is designed to maintain $\pm$ 5% accuracy for a maximum velocity change of 130 m/sec in 0.25 seconds in the natural environment. The step function response characteristics of the Maxometers were analyzed by review of wind tunnel test film data. The method of simulating the step function application of wind speed is described on page 5-7.

Response characteristics for test runs Nos. 19, 20 and 22 are shown graphically in Fig. 5-12. These data were obtained by a frame-by-frame analysis of the motion picture film for the S-2 Maxometer. Analysis of the E-1 unit showed very similar characteristics. The characteristics are generally that of an overdamped system as shown by Run 19 at 30 m/sec. However, at the higher velocities, additional dynamics are introduced. The oscillations are apparently caused by lag in the clutch engagement which allows direction change in the piston assembly. The force reversal is caused by the combined high inertia forces at contact with the high-rate spring and compression of air behind the piston which is not relieved rapidly enough by the orifice. After the clutch engages, at approximately 0.10 second, the orifice controls the rate of change in piston displacement until the final velocity is reached (at approx. 0.47 seconds).

For the overall system response approximately 80% of the final displacement is achieved in 0.125 seconds at the higher velocities. For the lower velocity (30 m/sec), 80% displacement is achieved in approx. 0.31 seconds.

Concluding observations of the Maxometer response characteristics are:

1. Although the step function response appears very good, the Maxometer is heavily damped for the 130 m/sec velocity change in 0.25 seconds condition. However, this response appears consistent with the analog simulation for the tornado condition (page 3-14). An increase in orifice diameter is recommended only if peak winds of less than 0.50 second duration are anticipated. This orifice diameter increase should be determined experimentally. Present orifice diameter is 0.020 inches (0.51 mm).

2. The response characteristics are very similar for the full velocity range. This is especially apparent in the 0.10 to 0.50 second time period, and for the higher velocities where the high rate spring is engaged (Runs 20 and 22).

3. For the step function input at velocities higher than $\simeq 30$ m/sec positive clutching does not occur until after 0.10 seconds. This does not appear detrimental to the Maxometer performance and appears adequate. However, decreased damping by increasing the orifice size may alter this condition and should be evaluated simultaneously with any orifice size change.

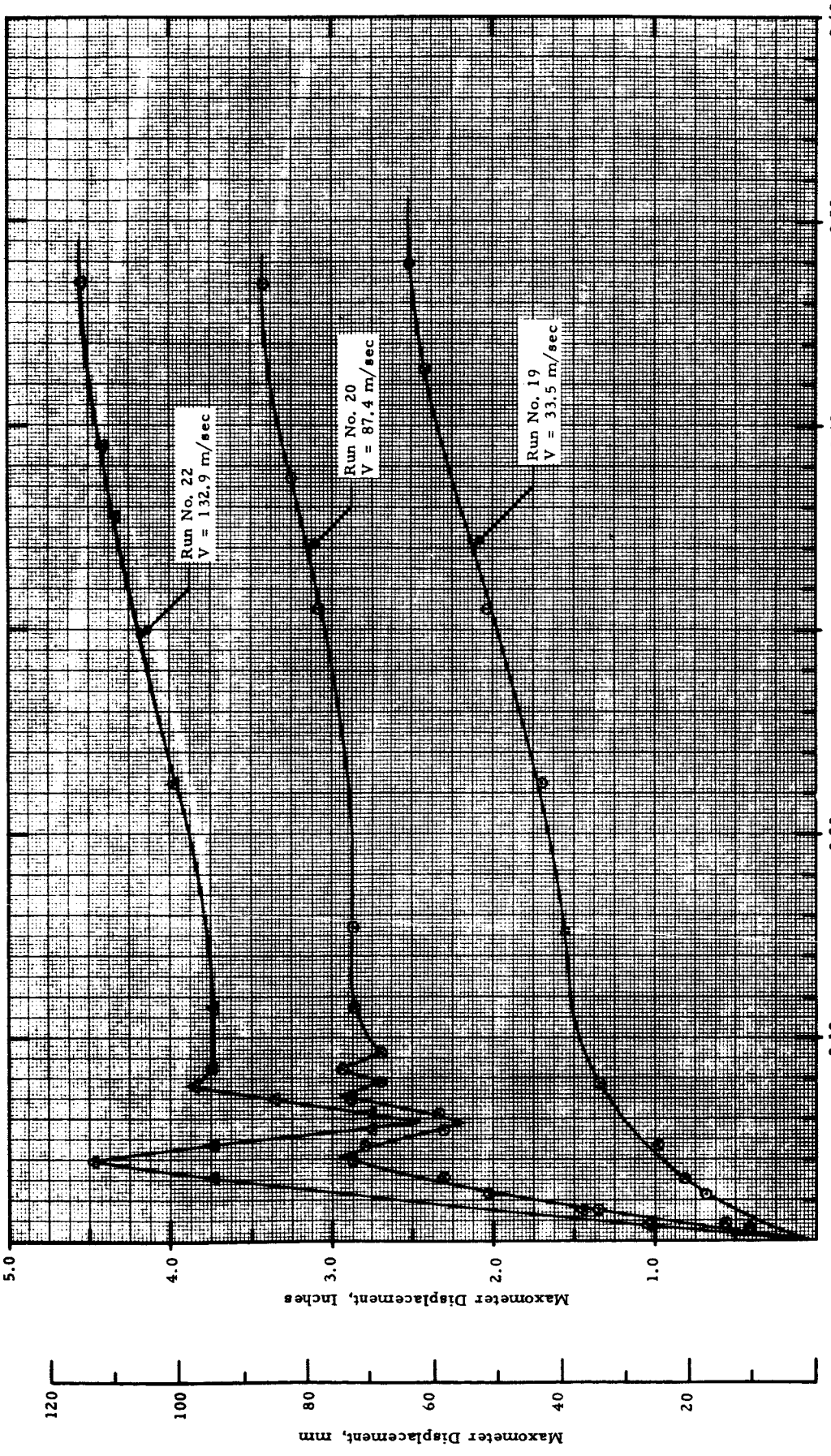

Fig. 5-12 - Maxometer Response Characteristics

Section 6
CONCLUSIONS AND RECOMMENDATIONS

As a result of the design, development and testing efforts involved in this program, it is concluded that the Maxometer concepts (Models S and E) are capable of meeting the specifications outlined in Section 2 of this report. Test data indicate that the Maxometer is capable of measuring dynamic pressures up to 200 lb/ft^2 (977 kg/m^2). This is equivalent to a maximum velocity of 205 m/sec at 1000°F (538°C) or 122.7 m/sec at 60°F (15.6°C). Dynamic response test data indicates that the Maxometer response is adequate if the peak wind speed pulse is 0.50 seconds or greater, and that the Model E weather-vaning response is adequate. Also, the test data indicate that the instrument is capable of meeting the velocity measuring accuracy of $\pm$ 5% of reading. The Maxometer low velocity threshold was specified at 8 m/sec at 60°F (15.6°C) and 14.7 psia (1013 mb). Test data indicated approximately a 16.5 m/sec at this temperature and pressure. However, this data is inconsistent with the laboratory calibration data, and the NASA-Langley wind tunnel personnel indicated that their data was subject to inaccuracies near 20 m/sec and below.

Also, as a result of the Maxometer design and development efforts, there were certain recommendations for further work to refine the Maxometer concept. This work involves minor design changes and further calibration testing as outlined below.

Design Changes

- For the Model S Maxometer, select al alternate material for the nose caps to reduce the fabrication costs. These nose caps should be capable of meeting the Model S high temperature environmental requirements.
- For Models E and S, devise a method for preventing excessive sagging of the high rate spring in the horizontal position. Also, provide a protective cover or shield over the ball clutch on the nose cap.

- For Models E and S, reduce the resolution error at high rate spring engagement by reducing the spring rate of the high rate spring, or by increasing the overall displacement and the low rate spring displacement prior to high rate spring engagement. (See Section 3.4.1.)

- For Models E and S, change hardened steel rod material. During environmental exposure of the first few Maxometers, it became apparent that the hardened steel rod, on both models (reference Fig. 3-3), cannot withstand adverse environmental conditions. The salt air, moisture, etc., environment severely corrodes the rods. Subsequently, it is recommended that future Maxometers be fabricated with a higher grade stainless steel or an equivalent treated material.

Further Testing

- Further wind tunnel calibration testing is recommended to evaluate the Maxometer low range characteristics. This should be accomplished in a tunnel facility with sufficient size to mount the Maxometer assembly and which has velocity accuracy of $\pm 1\%$ in the 1 to 10 lb/ft^2 dynamic pressure range.

- Further field and environmental testing is recommended to evaluate the Maxometer in its intended environment. This should include high and low temperature tests with simulated rain, snow and sleet conditions. Also, vibration tests should be conducted to evaluate limitations in this type of environment.

Section 7
REFERENCES

1. Hoerner, S. F., Fluid-Dynamic Drag, New Jersey, 1965.

2. Stephens, R., and A. Bates, Acoustics and Vibrational Physics, St. Martin's Press, New York, 1966.

3. Dunbar, A. S., "Lectures on Electromagnetic Scattering and Radar Cross Section," unpublished.

4. King, R., and T. Wu, The Scattering and Diffraction of Waves, Harvard University Press, Cambridge, Mass., 1959.

5. Kraus, J., Electromagnetics, McGraw-Hill, New York, 1953.

6. Kennedy Space Center, "Results of AS-503 Facilities and Environmental Measurements," TR 927, 30 January 1969.

7. Roark, R. J., Formulas for Stress and Strain, McGraw-Hill, New York, 4th Edition, 1965.

8. MacCready, Jr., P. B., and H. R. Jex, "Response Characteristics and Application Techniques of Some Meteorological Sensors," MRI 63, June 1963, p. 86.

9. Daniels, Glenn, et al., "Terrestial Environment (Climatic) Criteria Guidelines for Use on Space Vehicle Development, 1969 Revision," NASA TM X-53872, September 1969.

10. Phone conversation, P. T. Johnson of Lockheed/Huntsville and representative of Kinemotive Corp., J. Soehner Div., 12 May 1969, Subject: Nonlinear Springs.

11. Phone conversation, P. T. Johnson of Lockheed/Huntsville and Donald Wilkes of Rolamite, Inc., 19 May 1969, Subject: Rolemite Concept Invented by Mr. Wilkes.

12. Chironis, Nicholas P., "Fiendishly Simple Roller-Band Device Challenges Established Mechanisms," Product Engineering, 6 November 1967.

DISTRIBUTION

DIR
DEP-T
A&TS-PAT
A&TS-MS-H
A&TS-MS-IP
A&TS-MS-IL (8)
A&TS-TU, Mr. Wiggins (6)
PM-PR-M, Mr. Goldston

AD-S
Dr. Stuhlinger

S&E-COMP
Mr. Houston

S&E-ASTN
Mr. Moore

PM-MT-SR
Mr. Nybo

S&E-AERO
Dr. Geissler
Mr. Dahm
Mr. Reed
Mr. Kaufman (50)
Dr. Fichtl
Mr. O. Smith
Mr. R. Smith
Mr. W. Vaughan (5)
Mr. Turner
Mr. Camp
Dr. DeVries

Tech. & Sci. Info. Facility (25)
Box 33
College Park, Md.
Attn: NASA Rep. (S-AK/RKT)

NASA Headquarters
Washington, D. C. 20546
Ofc. of Adv. Res. & Tech.
Attn: W. Wilcox
F. Stephenson, Jr.

NASA Headquarters (Cont'd)
Ofc. of Space Science & Appl.
Attn: Dr. M. Tepper (2)

NASA - Kennedy Space Center, Fla.
Attn: J. Fulton
J. Claybourne
R. Clark
E. Amman
R. Bruns
L. Keene
R. Wilkinson
T. Michalek
G. Walter
W. Jelen
E. Scott

NASA-Langley Research Center
Attn: W. Reed, III
H. Tolefson
R. Henry
E. Polhamus
H. Wiley
E. Davenport

NASA-Manned Spacecraft Center
Houston, Texas 77058
Attn: D. Wade
R. Siler

Mr. George Ortiz
NASA-Manned Spacecraft Center
White Sands Missile Range Operations
P. O. Box MM
Las Cruces, N. M. 88001

Commander
Hdqs., Air Weather Service
Scott AFB, Ill. 62225
Attn: Dr. R. D. Fletcher
Tech. Library (3)

Ofc. of Staff Meteorologist
AFSC (SCWTS)
Andrews AFB
Washington, D. C. 20331

Mr. Paul F. Bikle
Dir., Flight Res. Center
NASA
P. O. Box 273
Edwards, Calif. 93523

National Hurricane Center
Univ. of Miami
P. O. Box 8286
Coral Gable, Fla. 33126
Attn: Mr. A. Samet
Mr. A. Sugg

Meteorological & Geoastrophysical
Abstracts
P. O. Box 1736
Washington, D. C. 20013

Air Force Cambridge Res. Labs.
Bedford, Mass. 01730
Attn: Tech. Library (3)
Mr. R. Leviton

Dr. O. Essenwanter
AMSMI-RRA, Bldg. 5429
U. S. Army Missile Command
Redstone Arsenal, Ala. 35809

Mr. Orville Daniel
PAWA/GMRD, AFMTC
MU-235, Tech. Library
Patrick AFB, Fla. 32925

Mr. John F. Spurling
NASA-Wallops Island, Va. 23337

Air Force Flight Dynamics Lab.
Air Force Systems Command
Wright-Patterson AFB, Ohio 45433
Attn: Mr. Neal Loving (FDTR)

Mr. Grady Harger
ESSA/Weather Bureau
Silver Springs, Md.

Mr. A. J. Krueger
Code 50
Naval Ordnance Test Sta.
China Lake, Calif. 93555

Mr. B. F. Walker
USAF, PGLW
Air Proving Ground Center
Eglin AFB, Fla. 32542

WEA
Air Force Flight Test Center
Edwards AFB, Calif. 93523

Mr. K. C. Steelman
AMSEL-RD-SM
U. S. Army Elec. Res. & Dev. Lab.
Ft. Monmouth, New Jersey 07703

Mr. H. D. Bagley
AMSMI-RRA, Bldg. 5429
Physical Sci. Lab.
Redstone Arsenal, Ala. 35809

Mr. A. L. Miller
AIR-5403
Naval Air Systems Command
Washington, D. C. 20360

Mr. R. M. Fenn
KXR, DOD Code 1232
U. S. Naval Weapons Lab.
Dahlgren, Va. 22448

Mr. H. Demboski
Code: 421
Ofc. of Naval Res.
Washington, D. C. 20360

Meteorological Division
U. S. Army Signal Res. & Dev. Labs.
Ft. Monmouth, N. J. 07703

Mr. Joseph Goldman
Inst. for Storm Res.
3812 Montrose Blvd.
Houston, Texas 77006

Dr. Arnold Court
17168 Septo St.
Northridge, Calif. 91324

NASA-Flight Res. Center
Edwards AFB, Calif. 93523
Attn: Mr. J. Ehernberger

National Center for Atmos. Res.
Boulder, Colorado 80302

Inst. for Environmental Res.
ESSA - Research Labs.
Boulder, Colorado 80302

Dr. Hans Panofsky
The Pa. State Univ.
503 Deitu Bldg.
Dept. of Meteorology
University Park, Pa. 16802

Dr. J. R. Scoggins
The Texas A&M Univ.
Dept. of Meteorology
College Sta., Texas 77843

R. A. Taft Sanitary Eng. Center
Public Health Service
4676 Columbia Parkway
Cincinnati, Ohio 45226

Meteorology Division
U. S. Army Dugway Proving Ground
Dugway, Utah 84022

Atmos. Sci. Lab.
U. S. Army Electronics Command
White Sands Missile Range, NM 88002

Dr. H. Crutcher
ESSA-National Weather Records Center
Asheville, NC 28801

Dr. Frank Gifford
Dir., Atmos. Diffusion Lab.
U. S. Weather Bureau, ESSA
Oakridge, Tenn. 38111

Mr. Manuel Armendariz
U. S. Army
Electronics Res. & Dev. Activity
White Sands Missile Range
Las Cruces, NM 88001

Mr. T. R. Carr
Code 3251, Box 22
Pacific Missile Range
Point Mugu, Calif. 93041

Ofc. of Staff Meteorologist
Air Force Eastern Test Range
Patrick AFB, Fla. 32925

Dr. Sidney Teweles (W14)
Chief, Data Acquisition Div.
Environmental Sci. Services Adm.
Weather Bureau
8060 13th St.
Silver Spring, Md. 20910

Mr. N. J. Asbridge
WTWU
Air Force Western Test Range
Vandenberg AFB, Calif. 93437

Mr. V. S. Hardin
AWSAE
Air Weather Service
Scott AFB, Ill. 62226

Mr. K. M. Nagler
Chief, Space Operations Support Div.
U. S. Weather Bureau, Essa
Silver Spring, Md. 20910

Mr. C. A. Olson
Code 7261
Sandia Corp. Sandia Base
Albuquerque, NM 87110

Mr. L. L. Sims
USAERDAA, Meteorology Dept.
U. S. Army Electronics Proving
Ground
Ft. Huachuca, Arizona 85613

SAMTEC
Air Force Western Test Range
Vandenberg AFB, Calif. 93437
Attn: Chief Meteorologist

Dr. Harrison Cramer (GCA)
P. O. Box 15009
Salt Lake City, Utah 84115

Dr. George H. Milly
Geomet, Inc.
326 East Mongtomery Ave.
Rockville, Md. 20850

Mr. Q. S. Dalton
Code 3069
Naval Ordnance Test Station
China Lake, Calif. 93555